



Water Resources Research



RESEARCH ARTICLE

10.1029/2023WR036995

Key Points:

- Nitrate removal rates were 86% higher with the artificial canopy present than the no canopy control experiments
- Maximum nitrate removal occurred at intermediate velocity (6 cms⁻¹) for both the canopy and no canopy control experiments
- Mixing, induced by the canopy-open water interface, enhanced open channel nitrate removal rates

Supporting Information:

Supporting Information may be found in the online version of this article.

Correspondence to:

A. T. Hansen, amy.hansen@ku.edu

Citation:

Waterman, B. R., & Hansen, A. T. (2024). Hydro-biogeochemical controls on nitrate removal: Insights from artificial emergent vegetation experiments in a recirculating flume mesocosm. *Water Resources Research*, 60, e2023WR036995. https://doi.org/10.1029/2023WR036995

Received 5 JAN 2024 Accepted 15 JUL 2024

Author Contributions:

Conceptualization: A. T. Hansen

Formal analysis: B. R. Waterman
Funding acquisition: A. T. Hansen
Investigation: B. R. Waterman
Methodology: B. R. Waterman,
A. T. Hansen
Project administration: A. T. Hansen
Supervision: A. T. Hansen
Visualization: B. R. Waterman
Writing – original draft: B. R. Waterman
Writing – review & editing:
B. R. Waterman, A. T. Hansen

© 2024. The Author(s).

This is an open access article under the terms of the Creative Commons

Attribution License, which permits use, distribution and reproduction in any medium, provided the original work is properly cited.

Hydro-Biogeochemical Controls on Nitrate Removal: Insights From Artificial Emergent Vegetation Experiments in a Recirculating Flume Mesocosm

B. R. Waterman¹ and A. T. Hansen¹

¹Department of Civil, Environmental & Architectural Engineering, CEAE, University of Kansas, Lawrence, KS, USA

Abstract Environments with aquatic vegetation can mitigate excess nitrogen (N) loads to downstream waters. However, complex interactions between multiple hydro-biogeochemical processes control N removal within these environments and thus complicate implementation of aquatic vegetation as a management solution. Here, we conducted controlled experiments using a canopy of artificial rigid emergent vegetation in a recirculating flume mesocosm to quantify differences in rates of mass transport and nitrate (NO₃⁻N) removal between the open channel-canopy interface across a range in nominal water velocities. We found NO₃⁻N removal rates were 86% greater with the canopy present compared to no canopy control experiments and were always greatest at intermediate velocity (6 cms⁻¹). With the canopy present, a hydrodynamically distinct mixing layer formed at the open channel-canopy interface, and resources, such as carbon (C), CN ratios, and dissolved oxygen, differed between open channel and vegetated canopy. The dimensionless Damköhler (Da) number indicated NO₃⁻N removal rates were reaction limited (Da << 1) for all canopy experiments, yet across all velocities NO₃⁻N removal was more reaction limited in the open channel than the canopy due to higher rates of mixing and less contact time with reactive surfaces. We found significant relationships between NO₃¬N removal rates and Da with hydrodynamic metrics (mixing zone width and Reynolds number, respectively), suggesting that NO₃⁻N removal in the presence of rigid vegetation can be enhanced by manipulating flow conditions. These findings demonstrate that rigid emergent vegetation-open channel interfaces create conditions conducive for NO₃⁻N removal and with effective management can improve overall water quality.

Plain Language Summary Persistent excess nitrate (NO₃⁻N) in surface waters is a major threat to water quality. Environments with aquatic plants, like wetlands, vegetated ditches or streams, can improve water quality by removing NO₃⁻N from water ways, yet reasons for increased removal capacity, especially under different flow conditions, are unclear. Using a controlled, yet realistic experimental set up, we investigated how flow conditions impact rates of mass transport and NO₃⁻N removal near model canopies of rigid emergent aquatic vegetation. We found that the rate NO₃⁻N is removed from the water is greater when the model vegetation is present, but regardless NO₃⁻N removal rates were greatest at intermediate velocity. When the canopy was present, the transport of water and resources occurred much faster than the removal of NO₃⁻N. We observed predictive relationships between flow conditions with removal rates and the ratio of mass transport to NO₃⁻N removal rate which can be useful for predicting or increasing NO₃⁻N removal in real environments. Our findings show the transformative role rigid aquatic vegetation can have in improving water quality within flowing waters, offering a promising pathway for sustainable water management.

1. Introduction

Excess reactive nitrogen (N) loading into natural ecosystems is deemed one of the most pressing environmental concerns of the Anthropocene (Rockström et al., 2009). An estimated 80% of anthropogenic N loading derives from the application of N-based fertilizer to terrestrial systems for increased agricultural productivity (Gruber & Galloway, 2008). The effects of excess N have been particularly detrimental for aquatic ecosystems, as N leaching from agrarian landscapes degrades water quality via eutrophication and hypoxia (i.e., algal blooms and dead zones) in both inland and coastal systems (Conley et al., 2009; Rabalais & Turner, 2019). Excess N also poses direct risks to human health, with exposure through drinking water linked to conditions such as blue baby syndrome and cancer (Temkin et al., 2019; Ward et al., 2018). Consequently, there is heightened interest in increasing N removal in aquatic ecosystems. However, widespread implementation of effective management strategies (e.g., riverine wetlands) is hindered in part by insufficient current understanding of interactions and

tradeoffs in flow and biogeochemical conditions with respect to N removal (Czuba et al., 2018; Kalinowska et al., 2023; Marion et al., 2014; Rudi et al., 2020).

Denitrification is the primary pathway for complete N removal in surface waters, particularly where nitrate is non-limiting (Birgand et al., 2007; Castaldelli et al., 2015; Kreiling et al., 2010; Seitzinger et al., 2007). This ubiquitous, microbially mediated oxidation-reduction reaction is carried out primarily by facultative heterotrophs, which utilize oxidized N (nitrate; NO₃⁻) as an electron acceptor when oxygen concentrations are low and depend on external electron donors such as organic carbon (C) (Birgand et al., 2007; Knowles, 1982). Denitrification rates can therefore be limited by the supply and ratio of reaction resources, NO₃⁻ and C, however the relationship between N and C on N removal rates are highly variable (Czuba et al., 2018; Johnson et al., 2012; Taylor & Townsend, 2010). As an example, the CN ratios for optimal N removal in natural aquatic environments can range from 1 (i.e., Hansen et al., 2016) to around 10 (i.e., Chen et al., 2017). The significance of CN ratios on N removal potentially reflects a "stoichiometric window" of resource requirements of the microbial processes that utilize N and C (i.e., constructive vs. destructive metabolism), whereas the variability in ratios suggests other controls, such as environmental conditions and C quality, are also important (Taylor & Townsend, 2010).

Emergent vegetation, such as found within riverine wetlands, drainage ditches or canals, directly removes N by assimilating reactive forms (NH₄⁺, NO₃⁻) into biomass or indirectly facilitates removal by creating conditions conducive for denitrification (Bachand & Horne, 1999; Bastviken et al., 2009; Kreiling et al., 2010; Nifong & Taylor, 2021; Soana, Gavioli, et al., 2018; Xia et al., 2020). For example, emergent vegetation provides reactive surface sites for biofilms and associated microbial communities (Levi et al., 2015). Rigid emergent vegetation also directly and indirectly contributes to water column dissolved oxygen (DO) dynamics that are crucial for denitrification. For example, rigid emergent vegetation can increase DO concentrations at sensitive interfaces (i.e., stems, detritus, sediment), from local flow and turbulence around stems or shoot-to-root transport, that could limit denitrifiers from utilizing NO₃⁻ (Soana, Fano, & Castaldelli, 2018; Philippot et al., 2013, respectively). However, DO replenishment can indirectly increase DO consumption via heterotrophic activity, ultimately lowering DO concentrations enough for denitrifiers to utilize NO₃ (Brune et al., 2000; Longhi et al., 2008; Zhang et al., 2014). Vegetation-oxygen dynamics are complex, and can vary drastically based on spatial and temporal scales, however the effects of emergent vegetation presence on improving denitrification as a whole are well documented (i.e., Bastviken et al., 2009; Kreiling et al., 2010; Castaldelli et al., 2015). Perhaps more significant for enhancing denitrification at larger scales (i.e., reach or watershed), rigid emergent vegetation provides optimal organic C quantity and quality (Hume et al., 2002; Lin et al., 2002; Sirivedhin & Gray, 2006; Wang et al., 2019) and alters hydrologic conditions to increase contact time with reactive surfaces (Holland et al., 2004; Kadlec & Wallace, 2009). At a watershed scale, riverine wetlands can be a strategy to decrease N concentrations and loads by increasing organic C concentrations and water residence time (Czuba et al., 2018; Hansen et al., 2018).

Aquatic interfaces (i.e., localized zones where flowing water encounters porous physical obstructions, such as sediments or biota) are locations of enhanced biogeochemical cycling due to the convergence of contrasting biogeochemical conditions and hydrodynamic transitions (Marion et al., 2014; Nikora, 2010; Zhao et al., 2022). Enhanced N removal at local scales can have cascading effects on improved water quality from ecosystem to regional scales (Covino, 2017), making interfaces highly studied for their outsized role in pollutant removal. For example, hyporheic zones are highly studied interfaces where N removal is highest when time scales of reactivity and hydrological connectivity are similar (Grant et al., 2018; Harvey et al., 2019).

Interfaces between open water and aquatic vegetation, specifically, exhibit contrasting gradients between complimentary resources and are locations of heightened mixing and mass transfer (Meftah et al., 2014; Nepf, 2012; White & Nepf, 2007). To briefly summarize hydrodynamics at this interface, water velocity is quickly attenuated within canopies while increased in the open channel due to shear created by the physical obstruction, resulting in a confined mixing layer between the two zones (Ghisalberti, 2009; Nezu & Sanjou, 2008; White & Nepf, 2007). Flow within and around rigid emergent vegetation has been highly studied to quantify and scale the physical processes (i.e., generation of turbulence, vortex instability, shear layer development at the interface) responsible for the high rates of momentum and mass exchange that occur across these interfaces (Caroppi et al., 2021; Nepf, 1999; Nezu & Sanjou, 2008; Truong & Uijttewaal, 2019; Unigarro Villota et al., 2023). Nevertheless, there has been minimal progress on incorporating mass transfer with biogeochemistry, specifically NO₃⁻N removal, despite the recognized potential of vegetation-induced mass exchange to improve overall water quality.

WATERMAN AND HANSEN 2 of 25



Water Resources Research

In this study, we investigated NO₃⁻ as N (hereafter NO₃⁻N) transport and removal near the interface between an artificial emergent vegetation canopy and open water by conducting a series of controlled experiments in a recirculating flume mesocosm. We tested three hypotheses: (a) total NO₃⁻N removal is enhanced by the presence of emergent vegetated canopies which facilitate exchange of DO, N, and dissolved organic carbon (DOC) between the canopy and open water, (b) total NO₃⁻N removal increases with velocity due to higher rates of mass transport within and between canopy and open channel, and (c) NO₃⁻N removal is subject to different hydrobiogeochemical controls between zones (i.e., reaction-limited in open channel vs. transport limited in canopy). A controlled experimental approach such as this can improve predictive understanding of NO₃⁻N removal in vegetated environments by leveraging recent scientific advancements in disciplines of both hydrodynamics and biogeochemistry.

2. Materials and Methods

Within the methods section, we describe the overall experimental design (Section 2.1) as well as specific data and analysis used to test each of the three hypotheses. The NO₃⁻N removal experiments with canopy and no-canopy (Section 2.2.3) were used to generate data needed to calculate NO₃⁻N removal rates (Section 2.3.1) to test the first hypothesis. For the second hypothesis, we used NO₃⁻N removal rates from only the canopy experiments (Section 2.3.1) coupled with mass transport rates (Section 2.3.2) derived from hydrodynamic experiments (Sections 2.2.1–2.2.2) to test if NO₃⁻N removal was enhanced by increased transport of resources between canopy and open channel. For the third hypothesis, again using only canopy experiments, we compared rates of mass transport (Section 2.3.2) and rates of NO₃⁻N removal (Section 2.3.1) to assess NO₃⁻N removal controls in open channel and canopy zones using a dimensionless number framework (Section 2.3.3). Details of experimental variables, units, and definitions are summarized in the Appendix (Tables A1 and A2).

2.1. Experimental Design and Setup

We used a recirculating flume mesocosm at the University of Kansas EcoFluids Laboratory to assess the influence of emergent vegetation on hydrodynamics and NO_3^-N removal (Figure 1). The flume was 0.47 m wide (B), 0.31 m tall, and 5.2 m long (L_f). Water from the flume emptied into a 1065 L reservoir and then recirculated through the flume mesocosm via a centrifugal pump. Polycarbonate honeycomb flow straighteners were placed at the front of the flume corridor to minimize entrance effects. Nominal streamwise velocity (U_{nom}) was controlled by adjusting valves on the return piping and measured prior to all experiments for 2 min upstream of the canopy at one third depth from bed using a SonTek acoustic Doppler velocimeter (ADV; SonTek YSI Incorporated, San Diego, CA, USA). Experiments were classified using U_{nom} (3, 6, or 9 cms $^{-1}$) which corresponds to low, intermediate and high velocity, respectively. The experimental velocities were selected to facilitate comparison to previous studies of N removal and fluid flow and are within ranges used for both experimental and field studies (e.g., Arnon et al., 2007; Caroppi et al., 2021; O'Connor & Hondzo, 2008; Soana, Gavioli, et al., 2018; Truong & Uijttewaal, 2019). A detailed list of variable notations and definitions can be found in Table A2 of the appendix.

The flume mesocosm was filled with tap water such that the flume corridor and reservoir water surfaces were level (depths of 0.23 and 1.3 m, respectively) at the onset of each experiment to avoid oxygenation. On the third day of each experiment, tap water was added to compensate for losses due to leaks and evaporation (0.2 m³; 10% of flume mesocosm volume). The water was amended with potassium nitrate (KNO₃) salt (approximately 5 g) to keep the concentration of the flume mesocosm consistent from before and after volume adjustments. Additionally, the reservoir water surface was capped with Styrofoam to limit aeration. A chiller (Penguin Chillers, Knoxville, TN USA) was used to regulate water temperature throughout the experiments.

The artificial vegetative canopy geometry emulated the geometry of live rigid emergent vegetation and followed previous hydrodynamic studies (Caroppi et al., 2021; Nepf, 1999; Unigarro Villota et al., 2023; White & Nepf, 2007). The canopy was half the flume width (0.23 m; b), 1.83 m long (L_c) and located 2.94 m distance from flume entrance, covering only a portion of the flume corridor to create flowing water of the open channel and canopy zones. This is similar to experiments emulating vegetation observed in wetlands, riparian patches, and floodplains (e.g., Caroppi et al., 2021; Truong & Uijttewaal, 2019). The canopy was composed of 0.0064 m diameter wooden dowels that extended out of the water column. The dowels were 0.013 m apart in both streamwise and lateral directions (dowel spacing; S) and secured into a 0.635 m thick perforated plastic baseboard for a total canopy density of 2555 dowels per m^{-2} . Using a dimensionless density, either by following Sehat

WATERMAN AND HANSEN 3 of 25

19447973, 2024, 8, Downloaded from https://agupubs.onlinelibrary.wiley.com/doi/10.1029/2023WR036995 by Amy Hansen , Wiley Online Library on [30/07/2024]. See the Terms and Conditions (https://on

Figure 1. Schematic of the flume mesocosm. (a) Side view shows sampling locations; three cross sections (XS; 1, 2, 3) and two depths (teal star and light brown circles). Velocity components are indicated by u and w (streamwise and vertical). (b) Top view shows water chemistry sample locations (green stars and periwinkle circles). Lateral water chemistry profile was collected at XS3, indicated by blue arrow. Dimensions are listed in text and in Appendix Table A1. Velocity components are streamwise (u) and lateral (v). (c) Example of dense rigid emergent vegetation (d) Images of how velocity profiles were measured with ADV. (e) Image to show water chemistry sampling for NO_3^-N removal experiments.

et al., 2023 (nm⁻² *d*stem thickness) or following Nepf, 1999 (d²/S²), the density for this study (0.22 or 0.25, respectively) is within the range of dense canopies of cattails, which range from 0.22 to 2.02 when using 140 nm⁻² and leave thickness of 4–10 mm (Glenn et al., 1995; Stevens & Hoag, 2000). Full mesocosm and canopy details can be found in Table A1.

The mesocosm sediment consisted of a hydric soil-sand mix that was added to approximately 5 cm depth along the entire flume corridor emulated natural bed roughness, which provided DOC and introduced a live microbial community (Figure 2). Wetlands soils (40 kg) from Lawrence, Kansas were mixed with commercial sands (Hydraulic Fracturing Sand, US Silica White) in a 1:2 ratio by volume. The sediment mix was amended (pre-experiment phase; Figure 2a) with particulate organic material (30 g total crushed leaves collected from Lawrence, KS) to ensure a slow, steady supply of DOC leaching from the sediments. This mixture resulted in a stable, ambient concentration of 5 mg/L DOC for the duration of all experiments. Additional C amendments were added prior to the NO₃⁻N removal experiments (Figure 2a; detailed in Section 2.2.3). The sediment mix underwent a series of wet-dry phases that led to the development of hydric soil as indicated by gley matrix and redox inclusions (Figure 2b; USDA NRCS, 2016) during which the hydrodynamic experiments were conducted. This soil development phase occurred over the course of 6 weeks prior to the NO₃⁻N removal experiments.

2.2. Sampling and Measurements

2.2.1. Water Velocity Sampling

Instantaneous velocity data was collected with a Nortek ADV in the streamwise, spanwise, and vertical directions, represented hereafter as u, v, w, respectively. The ADV employs Doppler shift principles to measure water velocity. Acoustic signals emitted by ADV receivers interact with suspended particles, causing frequency shifts corresponding to particle velocity, and hence water velocity. Given the presence of fine soils in our mesocosm, the water was naturally seeded with entrained soil particles, and the ADV measurements exhibited high signal-to-

WATERMAN AND HANSEN 4 of 25

19447973, 2024, 8, Downloaded from https://agupubs.onlinelibrary.wiley.com/doi/10.1029/2023WR036995 by Amy Hansen , Wiley Online Library on [30/07/2024]. See the Terms

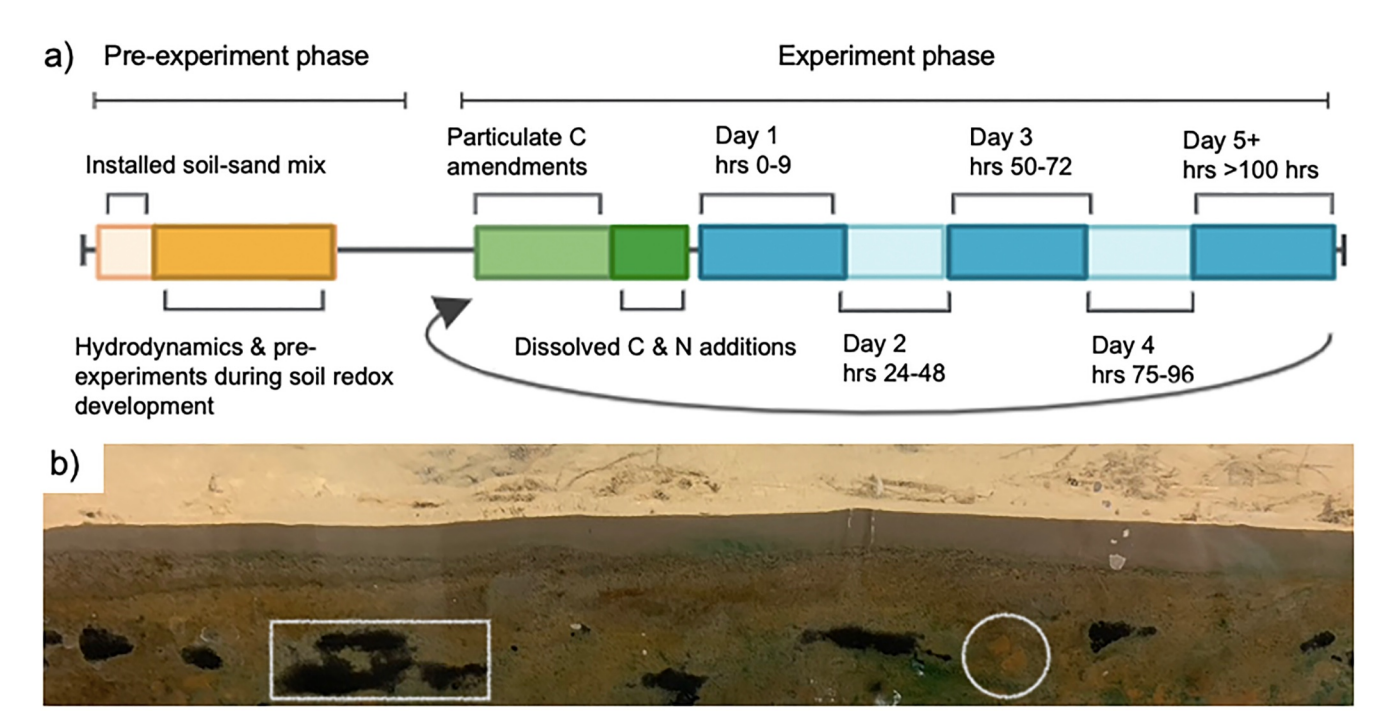


Figure 2. (a) Experimental timeline, black arrow shows the starting point of each experiment. (b) Image of soil profile in the flume mesocosm with rectangle and circle showing the redox indicators (black matrix and red-orange inclusions, respectively).

noise ratios (SNR > 15) without additional particle seeding. The ADV was mounted on a xz stage that moved laterally and vertically and position was measured to ± 1 mm. Data was collected at 200 Hz frequency for 1 minute at each sample location. Sufficient sampling duration (i.e., the time required to capture the largest eddies) was confirmed by comparing velocity data collected at one versus three-minute intervals for which there were no significant differences in mean and time-varying velocity components (Single factor ANOVA Table S1 in Supporting Information S1; p > 0.05), thus one-minute sampling time was used.

Lateral velocity profiles were measured at one third depth from the bed for three equally spaced cross sections (XS) along the canopy (0.41 m apart, L_{xs} ; Figure 1a). XS1 was the most upstream and XS3 was the most downstream profile. Each profile spanned from the open channel (OC) to canopy (VC) zones for the most of the flume width, 0.35 m, to avoid wall effects (B_{xs} ; Figure 1b). At each XS, select dowels were removable to allow for unimpeded ADV access across the interface for the velocity experiments (Figure 1d). The number of measurement locations per profile ranged from 18 to 26 (average 23), with more dense sampling locations near the canopy interface and at lower velocities due to the sensitivity of flow to canopy elements for these locations and conditions. Dowels were replaced following each measurement as the ADV was moved into the canopy to ensure flow was minimally disturbed for the subsequent measurements (Ikeda & Kanazawa, 1996; Unigarro Villota et al., 2023).

2.2.2. Water Velocity Data Processing and Calculations

Raw velocity data were filtered using WinADV software (USA Bureau of Reclamation) to remove measurements with correlation scores less than 80%, data spikes, and SNR ratios less than 15% (Unigarro Villota et al., 2023). The velocity data was first time-averaged using conventional Reynolds decomposition ($u = \overline{u} + u'$; $v = \overline{v} + v'$; $w = \overline{w} + w'$) where the instantaneous velocity component (e.g., u) is decomposed into the time-averaged velocity component (e.g., \overline{u}) and the fluctuating component (e.g., u'). Positive \overline{u} indicated water was moving in the direction of the main flow along the flume, positive \overline{v} indicated water was moving into the open channel, and positive \overline{w} indicated water was moving upward. The mean and fluctuating velocity components were then spatially averaged over each zone (e.g., $\langle \overline{u} \rangle_{oc} \langle u' \rangle_{oc}$) and for each cross-sectional profile to calculate

WATERMAN AND HANSEN 5 of 25

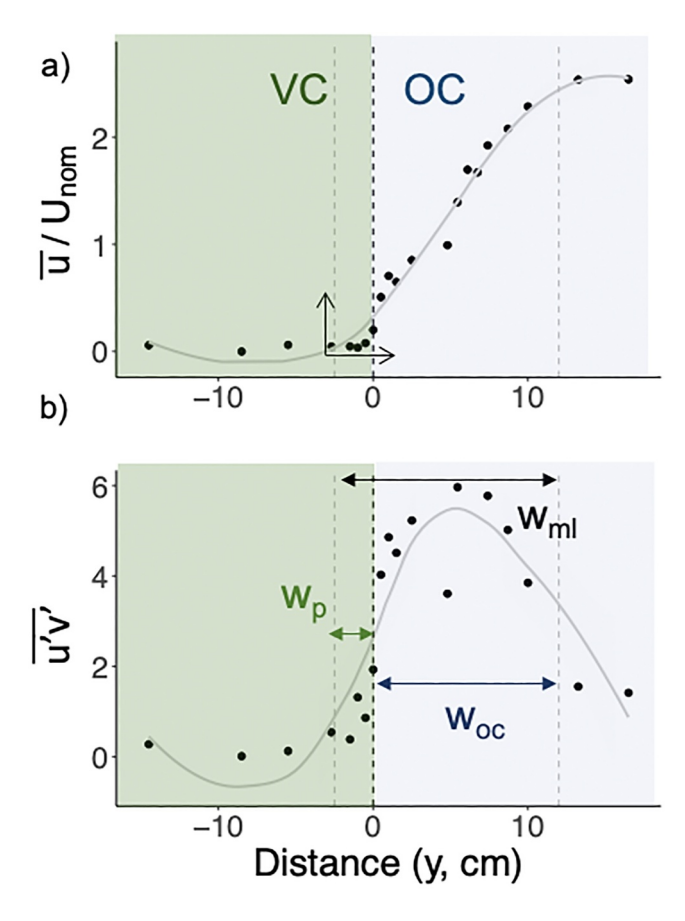


Figure 3. Example profile illustrating the mixing layer width (w_{ml}) , open channel portion of mixing layer (w_{oc}) , and shear extent into canopy (w_p) , in relation to streamwise velocity (a) and Reynold's stress data (b). Green zone is canopy, blue zone is open channel, black dashed line shows canopy interface, and gray dashed lines show boundaries of w_{ml} . Linear regression to find location of w_n shown in VC zone (a).

hydrodynamic metrics (detailed explanation in Section 2.3.2). Cross-sectional profiles of time-averaged velocity components are normalized to nominal experiment velocity $(\overline{u}/U_{nom},\overline{v}/U_{nom},\overline{w}/U_{nom})$.

The width of the mixing layer (w_{ml}) across the canopy interface was determined following (Ghisalberti & Nepf, 2004; Unigarro Villota et al., 2023) and as seen in Figure 3. The w_{ml} is defined as the distance between the nearest point where the mean velocity of the open channel is constant $(\langle \overline{u} \rangle_{oc})$ to the location where the lateral extent of momentum exchange (w_p; sometimes referred to as shear penetration) between the canopy and open channel occurs. The w_p was determined as the distance between the canopy interface and where Reynold stresses $(\overline{u'v'})$, the turbulent contribution to shear stress, decay to 10% of maximum, which generally corresponds with where the mean velocity within the canopy $(\langle \overline{u} \rangle_{vc})$ is constant (Ghisalberti & Nepf, 2005; Nepf & Vivoni, 2000; Unigarro Villota et al., 2023). The location of 10% max $(\overline{u'v'})$ along the profile was approximated using a linear regression (Figure 3a). The mixing layer (w_{ml}) was partitioned into the portion that is in the open channel (w_{oc}) and the portion that is in the canopy, (w_p) (Caroppi et al., 2021; Ghisalberti & Nepf, 2005). As the mixing layer extent was not definitively known until after all experiments ended, it was not possible to separate water chemistry using the mixing layer. Thus, water chemistry, NO₃⁻N removal rates, and dimensionless numbers are reported for two zones, canopy (VC) and open channel (OC), instead of the three zones used to report hydrodynamic results.

2.2.3. NO₃-N Removal Experiments

 ${
m NO_3}^-{
m N}$ removal experiments were conducted with the canopy installed in the flume and without the canopy (control) and at the same nominal velocities, ${
m U}_{
m nom}$, as hydrodynamic experiments, for a total of six experiments. Canopy experiments were carried out in the order of increasing ${
m U}_{
m nom}$ (Figure 2a). Control experiments were conducted 1 month after completion of canopy experiments in the order of intermediate, low, then high velocity. All experiments were conducted a week apart.

At the onset of each experiment, the mesocosm reservoir water was amended to an initial concentration of 5 mg/L $\rm NO_3^-N$ while particulate and dissolved forms of C were added to the canopy zone to an initial concentration of approximately 10 mg/L DOC. Specifically, 160 g of 1:4 glucose-corn meal mixture was evenly dispersed across the canopy zone (particulate), while a 1 L solution of glucose (40 g) and 200 mL solution of leaf leachate (approximately 1,200 mg/L DOC, CN ratio 40:1) was injected near the surface-water interface within the canopy zone (or where the canopy had been for the no canopy control experiments). C amendments were added only to the canopy zone to emulate field conditions of live emergent vegetation, which leaches DOC and contains litter (Hume et al., 2002; Longhi et al., 2008). The dissolved C amendment was used to quickly drive down dissolved oxygen (DO), and the particulate C amendment was used to sustain microbial populations and C concentrations over the duration of the experiments.

Water chemistry was assessed daily for up to 6 days (150 hr) during each experiment. For canopy experiments, water samples were collected from the open channel (OC) and vegetated canopy (VC) zones at the three XS, at one third depth (water column; WC) and at the sediment water interface (SWI), resulting in 12 samples daily. On the final day of each experiment, water samples were taken at one third depth along a lateral profile at XS3 to measure the concentration gradient across the OC to the VC (Figure 1b). The lateral profile was 0.3 m in width and spanned 0.15 m from interface in both directions (Figure 1b; blue arrow), and consisted of five sample locations that were equally spaced (0.08 m apart), with two samples taken from both the OC and VC and one at the interface, simultaneously collected from all five locations using a peristaltic pump (Figure 1f). For the control

WATERMAN AND HANSEN 6 of 25

com/doi/10.1029/2023WR036995 by Amy

experiments, samples were collected at only at XS3, at two lateral locations, and at both one third depth (WC) and at the SWI, resulting in only four samples daily.

Water chemistry samples were filtered immediately upon collection through 0.7 µm pore diameter, pre-ashed glass fiber filters (Whatman, Kent, UK). Samples for NO₃-N analysis were stored in acid-washed 60 mL Nalgene bottles and samples for dissolved organic carbon (DOC; non-purgeable organic carbon method) and total dissolved nitrogen (TDN) were stored in pre-combusted 24 mL glass vials. All samples were temporarily stored in the dark, on ice for the duration of daily sampling (1-3 hr) then transferred and stored until analysis at 4°C. Samples were analyzed for NO₃⁻ N within 24 hr using the Ultraviolet (UV) spectrophotometric screening method (Goldman & Jacobs, 1961) on Biotek Synergy LX Multi-Mode Reader (Agilent, Santa Clara, CA, USA). Samples for dissolved organic carbon (DOC; non-purgeable organic carbon method) and TDN were either analyzed immediately or acidified with 0.5 µm 2 M HCl and stored until analysis on a total organic carbon analyzer (TOC-L Shimadzu, Nakagyo-ku, Kyoto, Japan). The two sample storage approaches for TOC are acceptable according to EPA-RCA Method 9060A for Total Organic Carbon and were compared to validate that difference were negligible (ANOVA Table S2 in Supporting Information S1, p > 0.05). Temperature (T, °C), pH, conductivity (EC, μs/cm), total dissolved solids (TDS, ppm), and dissolved oxygen (DO, % and mg/L) were measured using handheld probes (Hanna HI98130, Combo pH/Conductivity/TDS Tester and YSI ProSolo Handheld Optical Dissolved Oxygen, respectively) that were calibrated daily following standard procedures. Sensor measurements were measured in both the WC and at SWI, consistent with water chemistry samples. Water chemistry results were temporally averaged over the duration of each experiment and spatially averaged by zone (e.g., $\langle \overline{DO} \rangle_{oc}$) and by canopy versus control (e.g., $\langle \overline{DO} \rangle_{Y.N}$). To ensure comparability across experiments, C and N were normalized to maximum concentrations for each experiment and are referred to as $\langle \overline{C/C}_{max} \rangle$ and $\langle \overline{N/N}_{max} \rangle$ hereafter.

2.3. Integrating N Removal and Hydrodynamics

2.3.1. Reaction Rates

First-order NO₃⁻N removal rate constants (κ_{rN_exp} ; s⁻¹) were estimated from the slope of the linear regression of the natural logarithm of the change in nitrate concentration over time (Equation 1; Figure S1 in Supporting Information S1). NO₃⁻N removal rates were calculated for each zone (OC and VC), XS (1, 2, 3), U_{nom} (3, 6, 9 cm/s), and canopy presence (Y/N).

$$\langle k_{rN} \rangle_{exp} = \frac{\ln(C_o) - \ln(C)}{\Delta t} \tag{1}$$

An Arrhenius temperature correction was applied to experimental removal rates (Equation 2; $\langle k_{rN} \rangle_{exp}$) to correct for an insufficiency with the chiller that resulted in high temperatures (35°C) for the latter part of the high velocity canopy experiments (100–160 hr). To ensure consistent comparison across experiments, all NO₃⁻N removal rates were adjusted from the average experimental temperature to standard conditions (25°C; 298.15 K) using the modified Arrhenius equation as follows:

$$\langle k_{rN} \rangle = \langle k_{rN} \rangle_{exp} e^{-\frac{\epsilon_e}{R} \left[\left(\frac{1}{\tau_{25}} \right) - \left(\frac{1}{\tau_{exp}} \right) \right]}$$
 (2)

where $\langle k_{rN} \rangle$ is the corrected N removal rate constant, ε_a is the activation energy of the reaction (60 kJ mol⁻¹), and R is the ideal gas constant (8.314 J mol⁻¹ K⁻¹) (Zheng et al., 2016). Both corrected and uncorrected rates are presented in the results, however only corrected removal rates were used in subsequent analysis and integrated with the hydrodynamics. Zonal removal rates were compared by the ratio of $\langle k_{rN} \rangle_{vc} / \langle k_{rN} \rangle_{oc}$, with lower values indicating higher removal rates in OC.

2.3.2. Mass Transport Rates

Using the velocity observations, the mass transport rate $\langle k_m \rangle (s^{-1})$ was defined as the ratio of turbulent kinetic energy (TKE; $m^2 s^{-2}$) to turbulent dissipation (ε ; $m^2 s^{-3}$) (Caroppi et al., 2021; Tang et al., 2023; Welty et al., 2000) and was calculated for both OC and VC zones (Equation 3).

WATERMAN AND HANSEN 7 of 25

$$\langle k_m \rangle = \frac{\langle TKE \rangle}{\langle \varepsilon \rangle} \tag{3}$$

Where lateral TKE and ϵ were calculated from velocity data, and then spatially averaged for each XS and within each zone as follows (Equations 4 and 5, respectively):

$$\langle TKE \rangle = \frac{1}{2} \left[\left\langle \overline{u}' \right\rangle^2 + \left\langle \overline{v}' \right\rangle^2 + \left\langle \overline{w}' \right\rangle^2 \right] \tag{4}$$

$$\langle \varepsilon \rangle = \frac{\langle \overline{u}' \rangle^{3}}{l} \left[\frac{sqrt \langle \overline{u}' \rangle^{2} + sqrt \langle \overline{v}' \rangle^{2} + sqrt \langle \overline{w}' \rangle^{2}}{l} \right]^{3}$$
 (5)

The length scales (*l*) were the dowel diameter (d) (Nepf, 1999; White & Nepf, 2007) for VC and the water depth (H) for OC (White & Nepf, 2007). Zonal rates were compared by the ratio of $\langle k_m \rangle_{vc} / \langle k_m \rangle_{oc}$, with values closer to 0 indicating greater transport in the OC.

2.3.3. Dimensionless Numbers

Dimensionless numbers are advantageous as they can simplify complex processes into transferable metrics and illuminate trade-offs between underlying hydro-biogeochemical mechanisms (Cheng & Basu, 2017; Gu et al., 2007; Musolff et al., 2017; Ocampo et al., 2006; Oldham et al., 2013; Pinay et al., 2015). In this study, the dimensionless Reynolds number (Re) was calculated for hydrodynamic zones and XS to understand how fluid flow conditions vary across and along the canopy. The dimensionless Damköhler number (Da) was also calculated for OC and VC zones and each XS to assess how controls on N removal varied between canopy and open channel and along the canopy length.

Re is the ratio of inertial to viscous forces in the flow (Equation 6) and was used to classify zonal flow conditions, laminar (Re < 3,000) or turbulent (Re > 3,000). Re was calculated by XS within three zones (OC, VC, and mixing layer) and is defined as,

$$Re = \frac{\langle \overline{U} \rangle l}{v} \tag{6}$$

where $\langle \overline{U} \rangle$ is temporally and spatially averaged streamwise velocity, v is the kinematic viscosity of water at 25°C (8.93E–7; m²s⁻¹), and l is the characteristic length scale (m) for each zone, which were the dowel diameter (d) for VC (Nepf, 1999; White & Nepf, 2007) and the water depth (H) for the OC and mixing layer following White & Nepf, 2007.

Da was calculated for the OC and VC, following Equation 7, to compare reaction rates of NO₃⁻N removal ($\langle \kappa_{r_N} \rangle$; Section 2.3.1) and rates of mass transport ($\langle k_m \rangle$; Section 2.3.2). Da <1 indicates that NO₃⁻N removal is limited by the molecular or microbial scale at which the reaction is occurring, $\langle \kappa_{r_N} \rangle$. When Da > 1, N removal is inferred to be limited by the supply, that is, mass transport, of reactants, $\langle k_m \rangle$.

$$Da = \frac{\langle \kappa_{r_N} \rangle}{\langle k_m \rangle} \tag{7}$$

Because the mixing layer location was not known a priori, $\langle \kappa_{r_N} \rangle$, and thus Da, were determined for OC and VC only, in contrast to Re, and by XS.

2.4. Statistical Analyses

All statistical analysis and data visualization were carried out in R (R Core Team, 2024). Data normality was assessed using the Shapiro test. Certain parameters (i.e., DO, DOC) were highly non-normal even after logarithmic transformation, thus relations between water chemistry data, U_{nom} (3, 6, 9 cm/s), sample location (i.e., by XS, OC or VC), or canopy presence (Yes/No) were assessed non-parametrically using pairwise Wilcox tests (first and second hypotheses). Simple linear regressions were used to assess DOC and NO_3^-N relationships (first

WATERMAN AND HANSEN 8 of 25

19447973, 2024. 8, Downloaded from https://agupubs.onlinelibrary.wiley.com/doi/10.1029/2023WR036995 by Amy Hansen , Wiley Online Library on [30.07/2024]. See the Terms and Conditions (https://onlinelibrary.wiley.com/doi/10.1029/2023WR036995 by Amy Hansen , Wiley Online Library on [30.07/2024]. See the Terms and Conditions (https://onlinelibrary.wiley.com/doi/10.1029/2023WR036995 by Amy Hansen , Wiley Online Library on [30.07/2024]. See the Terms and Conditions (https://onlinelibrary.wiley.com/doi/10.1029/2023WR036995 by Amy Hansen , Wiley Online Library on [30.07/2024]. See the Terms and Conditions (https://onlinelibrary.wiley.com/doi/10.1029/2023WR036995 by Amy Hansen , Wiley Online Library on [30.07/2024]. See the Terms and Conditions (https://onlinelibrary.wiley.com/doi/10.1029/2023WR036995 by Amy Hansen , Wiley Online Library on [30.07/2024]. See the Terms and Conditions (https://onlinelibrary.wiley.com/doi/10.1029/2023WR036995 by Amy Hansen , Wiley Online Library on [30.07/2024]. See the Terms and Conditions (https://onlinelibrary.wiley.com/doi/10.1029/2023WR036995 by Amy Hansen , Wiley Online Library on [30.07/2024]. See the Terms and Conditions (https://onlinelibrary.wiley.com/doi/10.1029/2023WR036995 by Amy Hansen , Wiley Online Library on [30.07/2024]. See the Terms and Conditions (https://onlinelibrary.wiley.com/doi/10.1029/2023WR036995 by Amy Hansen , Wiley Online Library on [30.07/2024]. See the Terms and Conditions (https://onlinelibrary.wiley.com/doi/10.1029/2023WR036995 by Amy Hansen , Wiley Online Library on [30.07/2024]. See the Terms and Conditions (https://onlinelibrary.wiley.com/doi/10.1029/2023WR036995 by Amy Hansen , Wiley Online Library on [30.07/2024]. See the Terms and Conditions (https://onlinelibrary.wiley.com/doi/10.1029/2023WR036995 by Amy Hansen , Wiley Online Library on [30.07/2024]. See the Terms and Conditions (https://onlinelibrary.wiley.com/doi/10.1029/2023WR036995 by Amy Hansen , Wiley Online Library (https://onlinelibrary.wiley.com/doi/10.1029/2023WR036995 by Amy Hansen , Wi

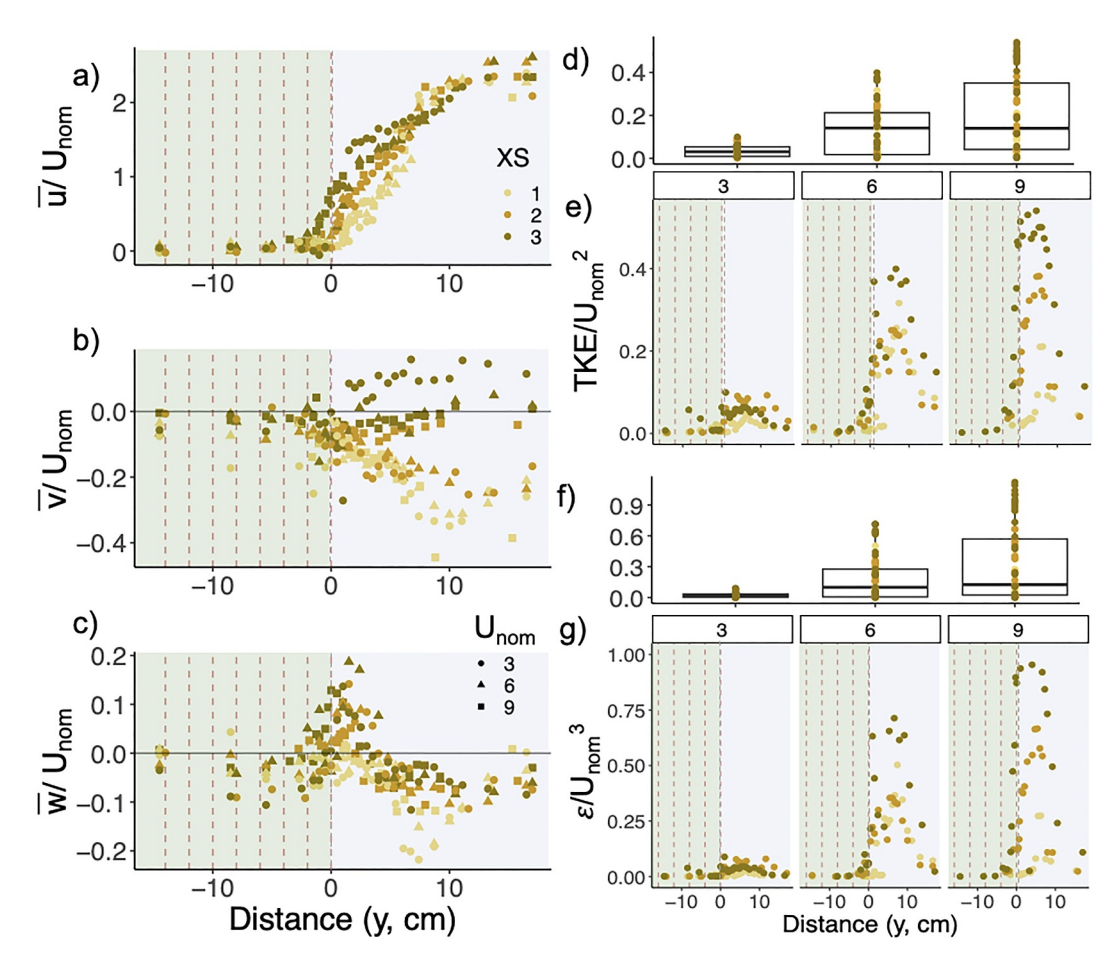


Figure 4. Cross-sectional profiles of streamwise (a), lateral (b), and vertical (c) velocity components. Cross sectional profiles of total kinetic energy (TKE) and eddy dissipation (ϵ) (g) normalized by nominal velocity (U_{nom}) squared and cubed, respectively. Panels (d) and (f) show box plots of normalized TKE and ϵ across all data for each U_{nom} . Marker shape indicates U_{nom} and color indicates cross-section location (front of canopy, XS1; middle of canopy, XS2; and XS3 for back of canopy). The background color on all panels except (d, f) indicates open channel zone (blue) or vegetated canopy zone (green; dashed lines).

hypothesis), as well as to identify predictive responses between hydrodynamics (e.g., Re_{oc} , w_{ml}) and removal (i.e., $\langle \kappa_{r_N} \rangle$) or Da, with R^2 values presented for each relationship and discussed in results (third hypothesis). Significant relationships between hydrodynamics and NO_3^-N removal rates or Da were identified using Spearman's Rho rank order correlation test (third hypothesis). Significance was assessed at $R^2 > |0.4|$ and P < 0.05 for all analysis.

3. Results

3.1. Hydrodynamics

3.1.1. Flow Profiles

For all velocity components, the shape of the profiles generally varied more with XS than with the nominal velocity (U_{nom}). Cross-sectional profiles of \overline{u}/U_{nom} rapidly decreased with distance from the open channel wall for each U_{nom} and XS (Figure 4a) and exhibited a hyperbolic tangent shape that is typical of mixing layers (Ghisalberti & Nepf, 2002; Nepf, 2012). For each U_{nom} and XS, values of \overline{u}/U_{nom} at the open channel wall were around two, that is, \overline{u} was nearly twice the respective U_{nom} , and near zero within most of the canopy.

The shape of the profiles of the lateral velocity component, \overline{v}/U_{nom} , were more variable with XS than \overline{u}/U_{nom} or \overline{w}/U_{nom} , as observed in Figure 4b. At XS1, \overline{v}/U_{nom} profiles were similar across each U_{nom} and consistently

WATERMAN AND HANSEN 9 of 25

negative at all locations indicating that water was routed into the open channel at the front boundary of the canopy. Profiles of \overline{v}/U_{nom} at XS2 exhibited similar patterns to XS1 for low and intermediate U_{nom} . In contrast, the shape of the \overline{v}/U_{nom} profile for the highest U_{nom} at XS2 was more similar to that for XS3 and had much smaller magnitude, although still negative. The \overline{v}/U_{nom} profile for low U_{nom} and at XS3 had positive values over the entirety of the open channel, indicating that water was routed from the open channel to the canopy. The intermediate and high U_{nom} profiles of \overline{v}/U_{nom} at XS3 exhibited a similar pattern to each other, with small but negative values for most of the profile, and with small, positive values in the outer portion of the open channel, indicating water was flowing toward the center of the open channel from the wall.

Cross-sectional profiles of the vertical velocity component, \overline{w}/U_{nom} , exhibited a consistent inflection point at the canopy interface regardless of U_{nom} (Figure 4c). Values of \overline{w}/U_{nom} in the middle of the open channel zone were negative for each XS and U_{nom} , indicating that flow was routed downward, that is, into the sediment. The magnitude of negative \overline{w}/U_{nom} was largest for XS1. Similarly, values within the middle of the canopy zone were negative and small for each XS and U_{nom} , indicating slow, downward moving water within the canopy. At the canopy interface, values were positive and nearly twice the open channel values, indicating flow was quickly being routed upward.

Cross sectional profiles of TKE/ U_{nom} and ϵ/U_{nom} were similar and peaked in open water near the canopy interface for each and U_{nom} (Figures 4e and 4g), indicating that maximum turbulence and mass transfer occurred in the open channel zone of the mixing layer near the interface (Liu et al., 2021; Truong & Uijttewaal, 2019). As U_{nom} increased, variability in TKE/ U_{nom} and ϵ/U_{nom} between XS increased (Figures 4d–4g). Average TKE/ U_{nom} and ϵ/U_{nom} were both highest for the intermediate U_{nom} , followed by the high U_{nom} and lowest for the low U_{nom} (Figures 4d and 4f, respectively).

3.1.2. Spatially Averaged Flow Conditions by Zone and Cross Section

In general, mixing layer Re, mixing widths, and TKE values are on the same order of magnitude compared to similar experimental set ups and flow conditions (e.g., Meftah et al., 2014; Caroppi et al., 2019, 2021; Tang et al., 2023; Table A3). For all velocities, Re indicated fully turbulent flow in the open channel and mixing layer (Re $_{\rm oc}$ & Re $_{\rm ml}$ > 3,000) and laminar flow within the canopy (Re $_{\rm vc}$ < 3,000; Table A3). Both Re $_{\rm oc}$ and Re $_{\rm ml}$ increased along the canopy length from XS1 to XS3, while Re $_{\rm vc}$ generally decreased from XS1 to XS3.

The mixing layer width (w_{ml}) increased from XS1 to XS3 for intermediate and high U_{nom} (67% and 49%, respectively). For low U_{nom} , w_{ml} increased from XS1 to XS2 (31% increase), yet slightly decreased in width from XS2 to XS3 (2% decrease). At XS1, the mixing layer did not extend into the canopy, as indicated by negative w_p values, for the low and intermediate U_{nom} . However, w_p decreased from XS2 to XS3 for low U_{nom} and increased from XS2 to XS3 for intermediate U_{nom} (42% and 60%, respectively). For high U_{nom} , w_p increased from XS1 to XS3 (113% increase). The open channel portion of the mixing layer, w_{oc} , increased about 20% from XS1 to XS3 for each U_{nom} . The w_{ml} , w_{oc} and w_p were all greatest for the intermediate U_{nom} , followed by high and then low U_{nom} .

Although there were three distinct zones according to velocity data (OC, VC, and mixing layer), TKE and ϵ were spatially averaged over just OC and VC, in order to be consistent with the zones used for water chemistry analysis and the evaluation of dimensionless numbers (Table A3). When averaged to compare zonal differences, open channel turbulent energy $\langle TKE \rangle_{oc}$ was always greater than canopy turbulent energy $\langle TKE \rangle_{vc}$ for all U_{nom} (101, 148, 100% greater from low to high U_{nom} , respectively). Conversely, canopy energy dissipation $\langle \epsilon \rangle_{vc}$ was greater than open channel energy dissipation $\langle \epsilon \rangle_{oc}$ (155, 90, 157% greater from low to high U_{nom} , respectively). From low to high U_{nom} , both $\langle TKE \rangle_{oc}$ increased and $\langle TKE \rangle_{vc}$ increased 140% on average, while both $\langle \epsilon \rangle_{oc}$ and $\langle \epsilon \rangle_{vc}$ increased 170% on average. When parsed by XS, $\langle TKE \rangle_{oc}$, $\langle TKE \rangle_{vc}$, and $\langle \epsilon \rangle_{oc}$ were greatest at XS2 for low U_{nom} and at XS3 for intermediate and high U_{nom} (Table A3). $\langle \epsilon \rangle_{vc}$ was greatest at XS3 for intermediate and high U_{nom} , and at XS1 for low U_{nom} .

3.1.3. Spatially Averaged Mass Transport Rates by Zone and Cross Section

Open channel mass transport rates ($\langle k_m \rangle_{oc}$), were greater than canopy mass transport rates ($\langle k_m \rangle_{vc}$) for all nominal velocities (U_{nom} ; Figure 5a). $\langle k_m \rangle_{oc}$ decreased as U_{nom} increased, while $\langle k_m \rangle_{vc}$ was greatest at high and low U_{nom} , and lowest at the intermediate U_{nom} (Figure 5a). The ratio of mass transport in the canopy compared to the open

WATERMAN AND HANSEN 10 of 25

nlinelibrary.wiley.com/doi/10.1029/2023WR036995 by Amy Hansen , Wiley Online Library on [30/07/2024]. See the Terr

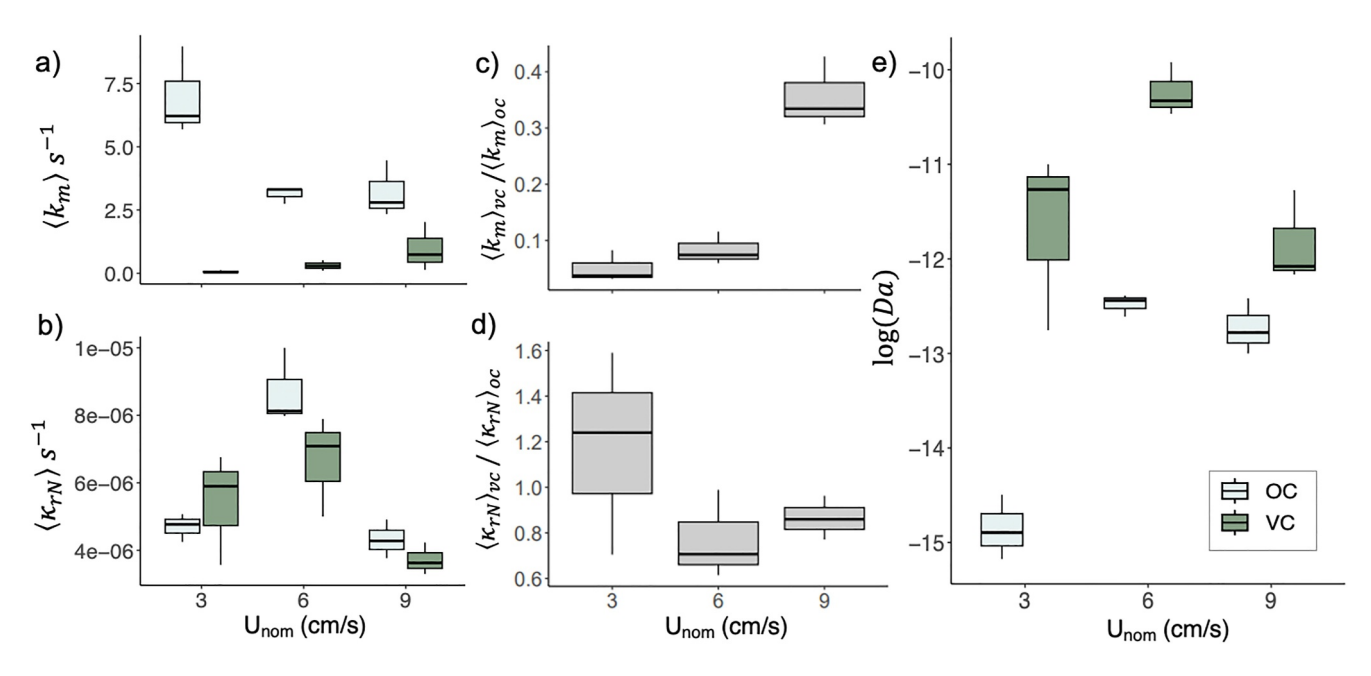


Figure 5. Boxplots of mass transport rates (a) and reaction rates (b) for each nominal velocity (U_{nom}) split by zone, open channel (OC) or vegetated canopy (VC). Ratio of VC to OC mass transport (c) and reaction rates (d). Damköhler number by zone and U_{nom} in log scale (e).

channel, $\langle k_m \rangle_{vc} / \langle k_m \rangle_{oc}$, increased with U_{nom} from 0.009, 0.1, to 0.39, demonstrating that mass transport was much higher in the open channel for low and intermediate U_{nom} but more evenly distributed between zones for the high U_{nom} (Figure 5b).

Cross-sectionally averaged mass transport rates showed that $\langle k_m \rangle_{XS1}$ was lower than $\langle k_m \rangle_{XS2}$ and $\langle k_m \rangle_{XS3}$ for low and high U_{nom} (Figure 6a). Conversely, $\langle k_m \rangle_{XS1}$ was greater than $\langle k_m \rangle_{XS2}$ and $\langle k_m \rangle_{XS3}$ for intermediate U_{nom} . Interestingly, for the lowest U_{nom} , mass transport rates increased along the whole canopy length $(\langle k_m \rangle_{XS1} < \langle k_m \rangle_{XS2} < \langle k_m \rangle_{XS3})$, while XS2 and XS3 were similar in magnitude at intermediate and high U_{nom} $(\langle k_m \rangle_{XS1} < \langle k_m \rangle_{XS3})$, suggesting flow conditions stabilized by XS2 at the higher velocities.

3.2. NO₃⁻N Removal Experiments

There were no significant differences for any water chemistry parameter by XS (Table S3 in Supporting Information S1), thus XS data were combined and water chemistry is reported by zone and U_{nom} only (Table A4). NO_3^-N removal rates did vary by XS, thus are reported by both zones and XS. Changes in NO_3^-N concentrations over time, from which removal rates were derived, can be visualized Figure S1 in Supporting Information S1. Significant differences are noted in text and on Figure 7, but for full statistical results, refer to Tables S3–S6 in Supporting Information S1.

3.2.1. Canopy Experiments: Water Chemistry by Nominal Velocity and Zone

All observed water chemistry parameters, dissolved oxygen (DO), DOC (referred to as C), nitrate (N), and C:N ratio notably varied by U_{nom} and zone (Figure 7). Water column $\langle \overline{DO} \rangle$ significantly increased with U_{nom} , from 78% saturation (±13), 87% (±10), 95% (±5) for low to high U_{nom} , respectively (Figure 7e). Across each U_{nom} , $\langle \overline{DO} \rangle_{oc}$ was higher than $\langle \overline{DO} \rangle_{vc}$, with significant differences by zone at low U_{nom} .

 $\langle \overline{C/C}_{max} \rangle$ increased with U_{nom} , 0.41 (±0.02), 0.45 (±0.17), 0.60 (±0.03) from low to high U_{nom} , respectively, with the highest significantly greater than low and intermediate U_{nom} (Figure 7f). $\langle \overline{C/C}_{max} \rangle_{oc}$ was lower than $\langle \overline{C/C}_{max} \rangle_{oc}$ for the low (0.40 < 0.42; significant difference) and high (0.60 < 0.61) velocities. In contrast, $\langle \overline{C/C}_{max} \rangle_{oc}$ was higher than $\langle \overline{C/C}_{max} \rangle_{vc}$ for intermediate U_{nom} (0.48 < 0.43). $\langle \overline{N/N}_{max} \rangle$ was significantly different across all U_{nom} , and lower for the intermediate U_{nom} (0.72) compared to the low and high U_{nom} (0.84 and 0.78, respectively) (Figure 7g). There were no significant differences between zones, however $\langle \overline{N/N}_{max} \rangle_{oc}$ was higher

WATERMAN AND HANSEN 11 of 25

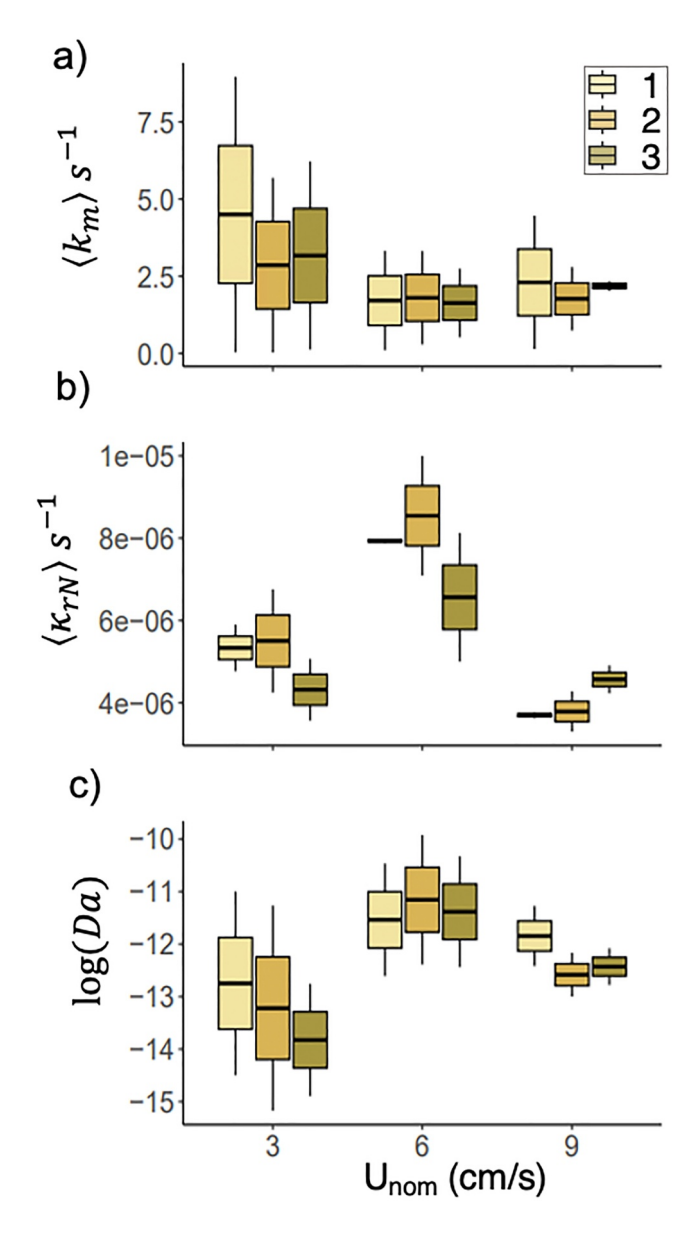


Figure 6. Boxplots of spatially averaged mass transport (k_m ; a), reaction rates (κ_{rN} ; b) and Damköhler number (c) for each velocity split by cross sections (XS) along the portion of the flume channel with the canopy, where XS1 is front, XS2 is the middle, and XS3 is the back of the flume channel where the canopy is located. Note Da is in log scale.

than $\langle \overline{N/N}_{max} \rangle_{vc}$ for low (0.85 > 0.82) and high U_{nom} (0.79 > 0.78), while $\langle \overline{N/N}_{max} \rangle$ for OC and VC were equal for intermediate U_{nom} (0.72).

Elemental ratios of C to N, $\langle \overline{CN}_{max} \rangle$, significantly differed across U_{nom} , increasing from 0.56 (±0.20), 0.64(±0.17), and 0.82 (±0.16) for low to high U_{nom} , consecutively (Figure 7h). By zone, $\langle \overline{CN}_{max} \rangle_{oc}$ was significantly lower than $\langle \overline{CN}_{max} \rangle_{vc}$ for low U_{nom} (0.52 ± 0.16 < 0.61 ± 0.25). Although results were not significant, $\langle \overline{CN}_{max} \rangle_{oc}$ was also lower than $\langle \overline{CN}_{max} \rangle_{vc}$ for high U_{nom} (0.79 ± 0.16 < 0.84 ± 0.15) but higher for intermediate U_{nom} (0.67 ± 0.22 > 0.60 ± 0.09).

There were significant differences in water chemistry based on sampling depth, water column (WC) versus SWI (Table S6 in Supporting Information S1). Specifically, $\langle \overline{CN}_{max} \rangle$ had significant differences depth, with $\langle \overline{CN}_{max} \rangle_{sw^i}$ greater than $\langle \overline{CN}_{max} \rangle_{w^c}$ (0.651 < 0.723, respectively). The inverse was true for $\langle \overline{DO} \rangle$, with $\langle \overline{DO} \rangle_{wc}$ greater than $\langle \overline{DO} \rangle_{swi}$ (85% > 8% respectively). Only $\langle \overline{DO} \rangle$ is separated by depth, with $\langle \overline{DO} \rangle_{wc}$ presented in Figure 7 and discussed further.

3.2.2. Water Chemistry by Canopy Versus Control Experiments

Water column $\langle \overline{DO} \rangle$, $\langle \overline{C/C}_{max} \rangle$, and $\langle \overline{CN}_{max} \rangle$, averaged across all U_{nom}, were significantly different between canopy and control experiments (Figures 7a, 7b, and 7d). Specifically, $\langle \overline{DO} \rangle_Y$ was significantly higher (86% saturation) compared to $\langle \overline{DO} \rangle_N$ (75% saturation) (Figure 7a). $\langle \overline{C/C}_{max} \rangle_Y$ was significantly lower and more variable for canopy experiments (0.51 ± 0.14) than $\langle \overline{C/C}_{max} \rangle_N$ (0.62 ± 0.26); Figure 7b). $\langle \overline{CN}_{max} \rangle_Y$ were lower than $\langle \overline{CN}_{max} \rangle_N$, with average values of 0.66 (±0.19) compared to 0.80 (±0.30), respectively (Figure 7d). Normalized N was similar across experiments, with $\langle \overline{N/N}_{max} \rangle_Y$ slightly higher (0.78 ± 0.09) than the control $\langle \overline{N/N}_{max} \rangle_N$ (0.77±; 0.08; Figure 7c).

Relationships between $\langle \overline{N/N}_{max} \rangle$ and $\langle \overline{C/C}_{max} \rangle$ varied greatly based on canopy presence (Figure 8). With the canopy, $\langle \overline{N/N}_{max} \rangle_Y$ and $\langle \overline{C/C}_{max} \rangle_Y$ were significantly and inversely related for all U_{nom} ($R^2 = 0.75, 0.69, 0.77$, respectively). For all control experiments, relationships between $\langle \overline{N/N}_{max} \rangle_N$ and $\langle \overline{C/C}_{max} \rangle_N$ were insignificant for each U_{nom} ($R^2 = 0.04, 0.06, 0.22$ from low to high velocity, respectively). Control experiment resources, $\langle \overline{N/N}_{max} \rangle_N$ and $\langle \overline{C/C}_{max} \rangle_N$, exhibited no relationship because $\langle \overline{C/C}_{max} \rangle_N$ did not vary.

3.2.3. NO₃⁻N Removal Rates

 NO_3^-N removal rates ranged from 3.3E–6 to 1E–5 s⁻¹ across all experiments and were well within previously reported rates for equivalent water depth (Bohlke et al., 2009). For canopy experiments, concentrations of both NO_3^-N and TDN decreased over time except for an initial increase in NO_3^-N at low U_{nom} within the canopy zone (Figure S1 in Supporting Information S1). Additionally, water column had higher concentrations than SWI (WC > SWI). Conversely for the control experiments, WC concentrations were generally lower than SWI, and TDN slightly increased while NO_3^-N slightly decreased (Figure S1 in Supporting Information S1).

In canopy present experiments, NO₃⁻N removal rates varied by zone (Figure 5c). For example, open channel removal rates, $\langle k_{rN} \rangle_{oc}$, were greater than canopy removal rates, $\langle k_{rN} \rangle_{vc}$, for intermediate (8.71E-6 > 6.66E-6 s⁻¹) and high U_{nom} (4.32E-6 > 3.72E-6 s⁻¹). However, at low U_{nom} $\langle k_{rN} \rangle_{vc}$ was greater

WATERMAN AND HANSEN 12 of 25

than $\langle k_{rN} \rangle_{oc}$ (5.41E-6 > 4.69E-6 s⁻¹). The ratio of OC to VC NO₃⁻N removal rates were all close to 1, indicating that removal was generally balanced between zones (Figure 5d). Ratios of zonal NO₃⁻N removal rates considerably decreased from 3 to 6 cms⁻¹ and slightly increased again at 9 cms⁻¹, suggesting that NO₃⁻N removal shifted from primarily occurring in the VC at low U_{nom} (ratio > 1) to greater removal in the OC at intermediate and high U_{nom} (ratio <1) (Figure 5d).

By XS (Figure 6b), $\langle k_{rN} \rangle$ for low and intermediate U_{nom} exhibited similar trends and were greatest at XS2 (5.51E-6 and 8.56E-6, respectively), followed by removal rates at XS1 (5.33E-6 and 7.94E-6, respectively) and then XS3 (4.32E-6 and 6.56E-6, respectively). For the highest U_{nom} , removal rates were greatest at XS3 followed by XS2 and XS1 (4.57E-6 > 3.79E-06 > 3.70E-06, respectively).

When averaged across U_{nom} and XS, NO_3 removal rates were 86% greater for the canopy experiments $\langle k_{rN} \rangle_{\gamma}$ than for control experiments, $\langle k_{rN} \rangle_{N}$ (the magnitude of the difference in black and gray points in Figure 9). For both canopy and control experiments, $\langle k_{rN} \rangle_{N}$ was greatest at intermediate U_{nom} . High and low U_{nom} removal rates similar with the canopy, $\langle k_{rN} \rangle_{\gamma}$, while low U_{nom} was greater than high U_{nom} for the control experiments, $\langle k_{rN} \rangle_{N}$. Temperature corrections decreased N removal rates by 19% for both $\langle k_{rN_{exp}} \rangle_{\gamma,Unom}$ and $\langle k_{rN_{exp}} \rangle_{N,Unom}$ (Figure 9; maroon vs. gray and black symbols).

3.3. Dimensionless Numbers Integrating Hydro-Biogeochemical Controls on NO₃¬N Removal

Across experiments with the canopy present, we observed Da << 1, indicating that NO_3^-N removal in our system was always reaction limited (Figures 5e and 6c). The small Da values stem from the stark differences in magnitude between rates of mass transport (from high frequency velocity data which occur on the scale of seconds), and zonal reaction rates (from changes in concentrations over time which occur on the scale of hours). However, we still observed meaningful trends in Da magnitude across the open channel and canopy zones. Da_{oc} was smaller than Da_{vc} across all velocities, however the difference between the zones decreased with velocity (U_{nom} ; Figure 5e). Da_{oc} increased from low to intermediate, then slightly decreased to high U_{nom} (3.68E-7 < 3.82E-6 > 3.04E-6, respectively) and minimally varied. Similarly, Da_{vc} increased from low to intermediate, but then considerably decreased to high U_{nom} (1.08E-5 < 3.67E-5 > 7.87E-6, respectively). Da_{vc} was more variable, particularly at low U_{nom} .

When calculated for each XS and compared by U_{nom} , there was no consistent trend from upstream (XS1) to downstream (XS3) (Figure 6c). At low U_{nom} , Da decreased from XS1 to XS3 (8.59E-6, 6.54E-6, 1.61E-6, respectively). Da at intermediate U_{nom} was more consistent along the canopy length, although Da did peak at XS2 (2.66E-5) and was similar at XS1 (1.59E-5) and XS3 (1.83E-5). Da at high U_{nom} was similar in magnitude yet inverse in pattern along canopy to intermediate U_{nom} , with Da decreasing from XS1 to XS2 and increasing to XS3 (8.39E-6 > 3.73E-6 < 4.25E-6, respectively). Da variability decreased with increasing U_{nom} .

From the Spearman correlation matrix of all hydrodynamic metrics, NO₃⁻N removal rates, and dimensionless numbers (Figure S2 in Supporting Information S1), we observed a significant relationship between open channel removal rates $\langle k_{rN} \rangle_{oc}$ with the open channel portion of the mixing zone width (w_{oc}, $R^2 = 0.73$; Figure 10c) and between Da_{oc} and Re_{oc} ($R^2 = 0.74$; Figure 10a).

4. Discussion

Multiple lines of evidence demonstrate that canopies of rigid emergent vegetation in flowing water ways provide ideal hydro-biogeochemical conditions conducive for enhanced rates of NO_3^-N removal. Section 4.1 examines the validity of the first hypothesis and explores why the canopy presence increased NO_3^-N removal compared to no canopy control, integrating hydrodynamic results (Sections 3.1.1–3.1.2) and N removal experiments (Sections 3.2.1–3.3.3). The second hypothesis is assessed in Section 4.2, which focuses on canopy experiments only and discusses the relationship between velocity (U_{nom}), mass transport rates (k_m), and NO_3^-N removal (κ_{rN} ; Sections 3.1.2–3.1.3, and 3.2.3, respectively). The third hypothesis is explored in Section 4.3, which discusses what the relationships between NO_3^-N removal rates and hydrodynamic metrics indicate about hydrobiogeochemical controls on NO_3^-N removal within the canopy and open channel (Sections 3.2.3 and 3.3) and how to leverage these findings outside of the experimental bounds of this study. Finally, Section 4.4 puts the results of this study in context of real systems, again integrating results from Sections 3.1 and 3.2, and discusses how vegetation management could be leveraged to improve N removal efficiency at larger scales. Throughout all

WATERMAN AND HANSEN 13 of 25

19447973, 2024, 8, Downloaded

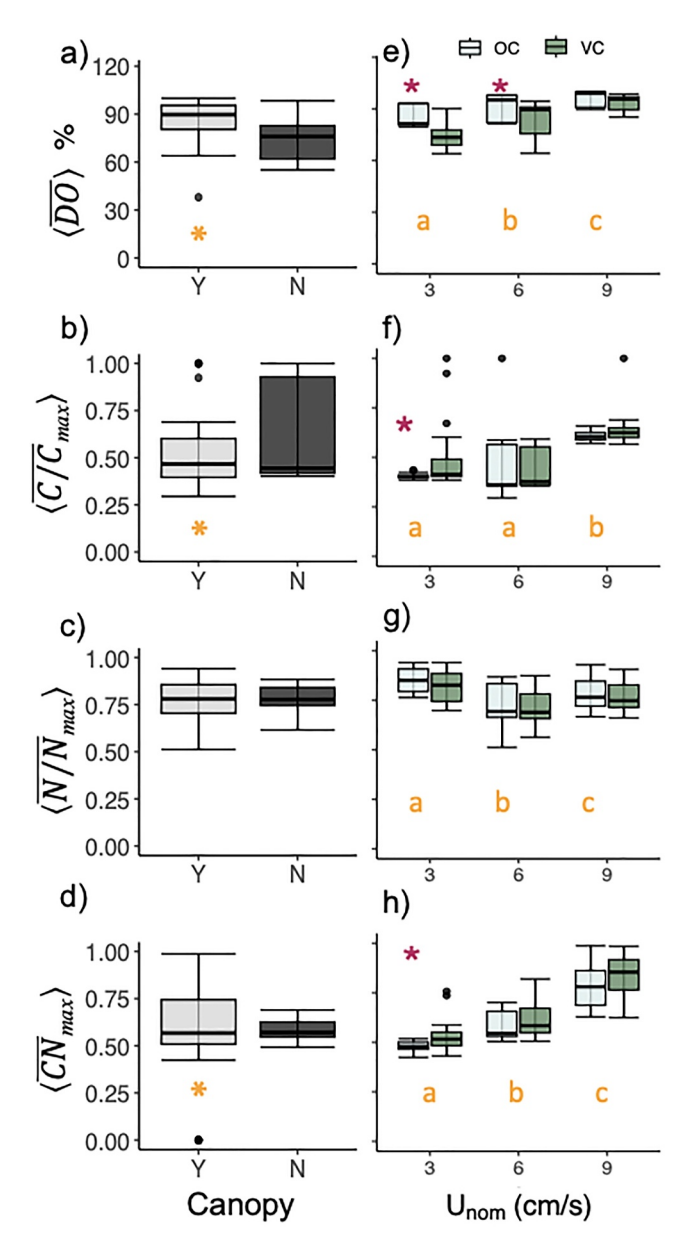


Figure 7. Water chemistry grouped by canopy presence (a–d; Y for yes and N for no canopy). Water chemistry from canopy experiments compared across nominal velocity ($U_{\rm nom}$) and grouped by zone (e–h). Orange (lighter colored) asterisks and letters (abc) indicate significant differences by canopy presence and $U_{\rm nom}$ respectively. Maroon (darker colored) asterisks indicate significant differences between zones. Boxplots illustrate 0.25, 0.5 (median), and 0.75 inter quantile ranges, while text and Table A4 describe the mean and standard deviations.

discussion sections, remaining knowledge gaps are presented that should be explored before implementing rigid emergent aquatic vegetation as a viable, and predictable, method for enhancing NO₃⁻N removal in real-world systems.

4.1. Canopies of Artificial Vegetation Enhance Overall NO₃⁻N Removal

An interplay of hydro-biogeochemical mechanisms contributed to the observed 86% greater $\mathrm{NO_3}^-\mathrm{N}$ removal with the canopy present compared to the no canopy control. From a hydrodynamic perspective, canopies of emergent vegetation alter velocity and enhance mixing (i.e., Nepf, 2012; Figure 4). Here, with the canopy present we observed that the hydrodynamics of the open channel and canopy zones varied drastically (Figure 4). The open channel near the interface was subject to enhanced mixing, as observed by the nearly double streamwise velocity (Figure 4a) and 100%-150% greater TKE than within the canopy (Figures 4d and 4f; Table A3). Conversely, the canopy was dominated by laminar flow conditions (Table A3), dispersion and viscous drag ($\mathrm{Re_{vc}} < 200$) (Nepf, 1999; Sabokrouhiyeh et al., 2017).

From a biogeochemical perspective, differences in NO₃⁻N and DOC concentrations for canopy and control experiments suggest that the ratio between the denitrification-limiting resources (DOC and NO₃⁻N) was modulated by the canopy presence (Figures 7b-7h, and 8). The significant differences in normalized DOC concentrations (C/C_{max}) and CN ratios (Figures 7b and 7d) suggest that the rate at which DOC and NO₃⁻N were released varied between canopy and control experiments. In both canopy and control experiments, DOC was injected directly into the canopy zone to emulate vegetative conditions. When the canopy was present, DOC was slowly released over the course of each canopy experiment. In contrast, DOC in the control experiments was quickly mixed throughout the system. For both the canopy and control experiments, NO₃⁻N was sourced from the flume reservoir and recirculated through the mesocosm predominantly in the open channel. As the canopy-derived DOC and open channel-transported NO₃⁻N were mixed between zones in the canopy experiments, direct controls on NO₃⁻N removal through denitrification were combined over longer timescales, as opposed to the no canopy control, supporting higher rates of NO₃⁻N removal. This canopy-modulated resource mixing can be observed by DOC-NO₃⁻N stoichiometry (Figure 8). For the canopy experiments, NO₃⁻N was significantly and inversely dependent on DOC (Figure 8). Conversely, there was no significant DOC-NO₃⁻N relationship in the no canopy control experiments. The inverse relationship between NO₃⁻N and DOC with the canopy is similar to what is observed in other aquatic ecosystems, indicative of microbial controls on resource stoichiometry (Taylor & Townsend, 2010).

Another crucial component of enhanced N processing in vegetative canopies and similar interfaces is the presence of biogeochemically reactive surfaces (Arnon et al., 2007; O'Connor & Hondzo, 2008; Soana, Gavioli, et al., 2018). Although the present work did not directly quantify biofilms, biofilms were

observed on canopy dowels and likely contributed to NO_3 ⁻N removal. Previous research has shown that biofilms on vegetation can increase N removal by enhancing microbial activity (Castaldelli et al., 2015; Soana, Gavioli, et al., 2018).

The findings of this study are consistent with our first hypothesis and contribute to the growing body of evidence for vegetation as a solution to degraded water quality by facilitating N removal (e.g., Castaldelli et al., 2015; Kalinowska et al., 2023; Rowiński et al., 2018; Soana, Gavioli, et al., 2018). Denitrification was assumed to be the dominant N removal process of our flume mesocosm. NO₃⁻N was directly added and the similarities in TN and

WATERMAN AND HANSEN 14 of 25

19447973, 2024, 8, Downloaded from https://agupubs.onlinelibrary.wiley.com/doi/10.1029/2023WR036995 by Amy Hansen , Wiley Online Library on [30/07/2024]. See the Terms

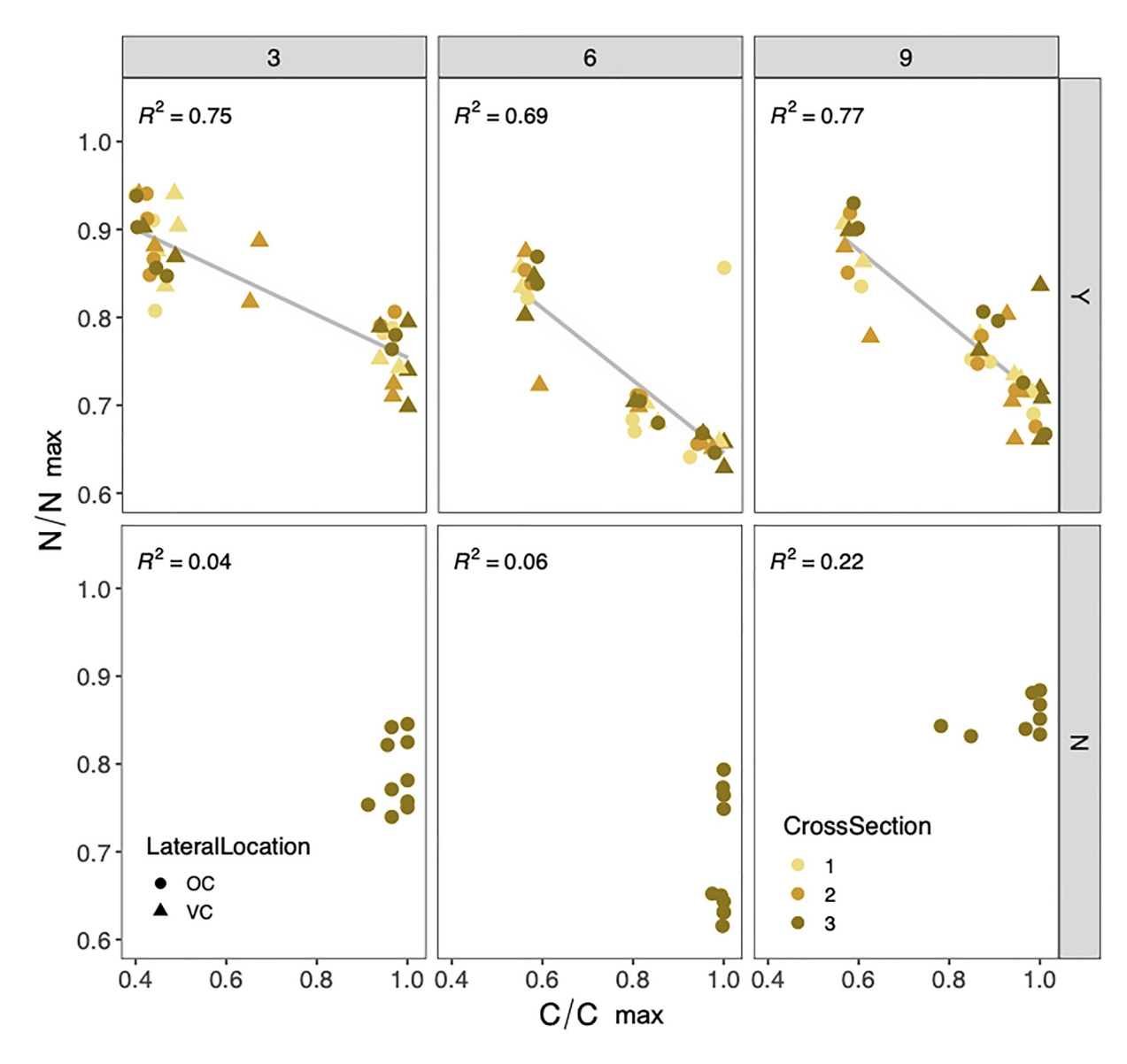


Figure 8. Relationships between $\langle \overline{N/N_{max}} \rangle$ and $\langle \overline{C/C_{max}} \rangle$ by U_{nom} (3,6,9 cms⁻¹) and canopy (Y) versus control (N). Point color indicates XS and shape indicates zone (OC or VC).

 NO_3 N suggest NO_3 N was non-limiting and the dominant form of N. However, denitrification end-members were not measured, so it is uncertain whether NO_3 N was completely removed as N_2 , partially removed as a denitrification intermediate (e.g., nitrite, nitrous oxide), or even reduced via dissimilatory nitrate reduction to ammonium (DNRA; Tiedje, 1988). However, in studies with similar water velocities and rigid emergent vegetation (live and dead), complete denitrification was shown to be the dominant pathway by comparing changes in inorganic N and N_2 production (e.g., Castaldelli et al., 2015; Castaldelli et al., 2018). The experiments herein were designed to emulate, yet simplify field conditions in order to test the hypothesis that the canopy presence, through the physical obstruction alone, enhances rates of NO_3 N removal. Future studies should add complexity, for example, by using live vegetation or by coupling available N-tracking methods (e.g., DIN budgets, DON/biomass, N_2 accumulation) to confirm removal pathways.

4.2. Trends in NO₃-N Removal Rates With Mass Transport and Nominal Velocity

 NO_3 N removal did not increase with rates of mass transport, $\langle k_m \rangle$, or nominal velocity (U_{nom}) , as expected with our second hypothesis. In fact, our results demonstrate that $\langle k_m \rangle$, as defined here by rate of turbulent energy

WATERMAN AND HANSEN 15 of 25

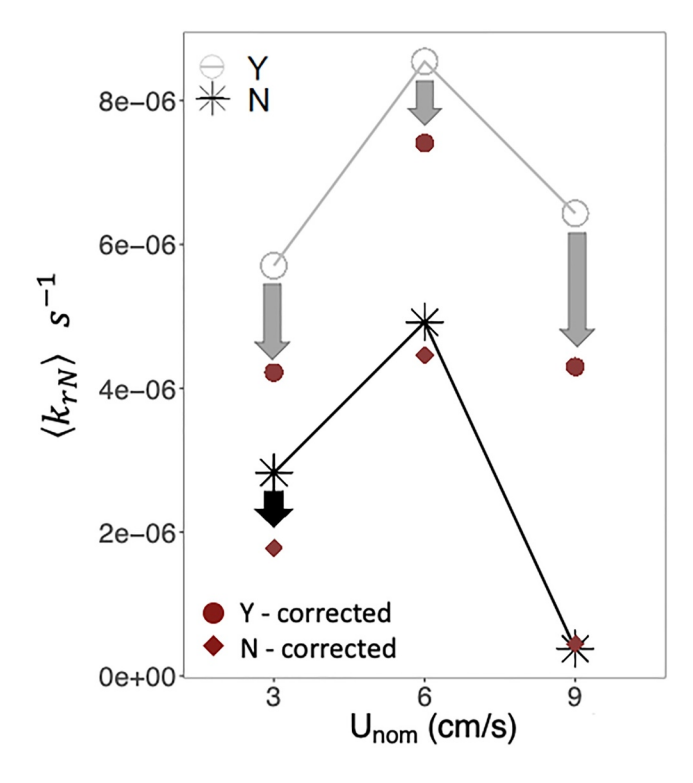


Figure 9. Experimental nitrate removal rates $\langle k_{rN_exp} \rangle$ with the canopy (gray, open circles) and for the no canopy controls (black asterisks) by nominal velocity (U_{nom} ; averaged across the three XS). The gray and black arrows pointing to the red markers show how temperature correction shifted rates $\langle k_{rN} \rangle$ for canopy and control experiments, respectively.

production to dissipation, decreased with increasing U_{nom} (Figures 5a and 6a). At low U_{nom} , more energy is generated by the canopy than energy dissipated by the canopy $(\langle k_m \rangle_{oc} > \langle k_m \rangle_{vc})$. The difference, or energy imbalance, between canopy and open channel zones decreased as U_{nom} increased (Figures 5a and 5c). This suggests that mixing between canopy and open channel zones actually increased with U_{nom} . Moreover, at low U_{nom} , $\langle k_m \rangle$ was more variable along the canopy length, while at intermediate and high U_{nom} , $\langle k_m \rangle$ was more consistent along the canopy length (Figure 6a). This result agrees with hydrodynamic literature that turbulent kinetic energy production and canopy dissipation become more balanced with distance downstream (Ghisalberti & Nepf, 2004; Meftah et al., 2014).

The nonlinear relationship between U_{nom} and N removal (Figure 9) is consistent with observations from experiments investigating hyporheic mixing on N removal (Arnon et al., 2007; O'Connor & Hondzo, 2008). Specifically, the conditions that maximize mixing between the distinct resources in the two zones (DOC in canopy, NO₃⁻N in open channel) yet minimize destructive effects of high velocity flows (scour and expansive oxic zones) resulted in the highest NO₃⁻N removal rates. For the low U_{nom} experiment, OC and VC were significantly different in DO, DOC, and CN (Figures 7e, 7f, and 7h), and had the lowest rates of NO₃⁻N removal (Figure 9). As U_{nom} increased to intermediate velocity, the mixing of chemically distinct water from the OC to VC could have increased heterotrophic activity at the interface by bringing DO into the DOC-rich canopy (Figures 7h and 7a respectively), simultaneously increasing heterotrophic activity at the interface and NO3-N removal in the canopy (O'Connor & Hondzo, 2008). Increasing U_{nom} to 9 cms⁻¹, however, had diminishing effects on NO₃⁻N removal as DO was replenished further into the canopy and faster than drawdown occurred, allowing for aerobic respiration to dominate over anaerobic processes such as denitrification (Arnon et al., 2007). At the highest U_{nom} , we observed similar DO conditions between

the two zones (Figure 7e), indicating expansive oxic zones, and low NO₃⁻N removal rates (Figures 5a and 9) to support this. Higher and more evenly distributed DO concentrations between the two zones was likely caused by the high turbulence generated just outside the canopy interface (Figure 4g), which would have entrained more oxygen from the air (Tseng & Tinoco, 2020) compared to the canopy zone. The canopy-induced entrainment of DO at the interface can also explain why the control experiments had lower DO concentrations on average compared to canopy experiments (Figures 7e and 7a respectively).

Our results suggest that open channel flow conditions and canopy reactivity were most balanced in terms of enhancing NO₃⁻N removal at intermediate U_{nom} (6 cms⁻¹; Figures 5b and 9). Similarly, Soana, Gavioli, et al. (2018) found N removal in presence of stems of emergent vegetation increased with velocity up to 6 cms⁻¹. Here, U_{nom} reached 9 cms⁻¹, and NO₃⁻N removal decreased (Figure 9). Enhanced mixing of resources with increasing U_{nom} can create a less biogeochemically active or distinct canopy zone from the open channel, resulting in less NO_3 ⁻N removal by the canopy due to the diminishing effects of DO or scour mentioned previously. The transition from higher $\langle k_{rN} \rangle_{vc}$ than $\langle k_{rN} \rangle_{oc}$ at low U_{nom} to greater $\langle k_{rN} \rangle_{oc}$ then $\langle k_{rN} \rangle_{vc}$ at higher U_{nom} supports diminishing canopy reactivity with higher U_{nom} (Figure 5b). Lateral profiles of water chemistry sampled on the last day of each canopy experiment further support this by showing greater changes in normalized NO_3 ⁻N concentrations across the open channel-canopy interface at intermediate U_{nom} compared to low and high U_{nom} (Figure S3 in Supporting Information S1). These results suggest that ecosystem services, such as NO_3 ⁻N removal, can be optimized by balancing resource replenishment (i.e., mass transport) with preserving biogeochemical conditions of canopies of rigid vegetation in flowing water ways.

4.3. Dimensionless Numbers Indicate Different Controls on NO_3 ⁻N Removal Between Open Channel and Canopy

The differences in Da magnitude and trends between open channel (OC) and canopy (VC) zones (Figures 5e and 10a and 10b) elucidate how hydro-biogeochemical controls on NO₃⁻N removal differ across the open channel-

WATERMAN AND HANSEN 16 of 25

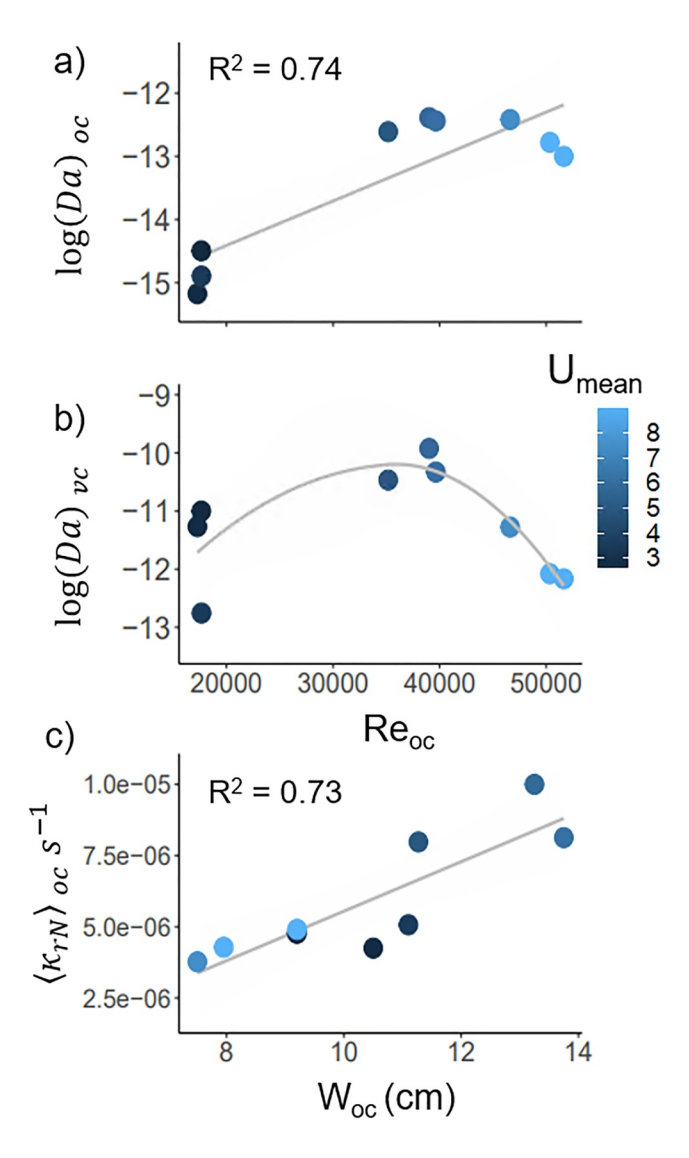


Figure 10. Relationships between zonal Da (OC and VC) and open channel Reynold's number (Re_{oc}) (a, b, respectively) and between open channel N removal rate ($\langle \kappa_{rN} \rangle$) with open channel mixing layer width, w_{oc} (c). Color represents mean streamwise velocity (cms⁻¹). Dimensionless numbers were calculated for canopy experiments only, at each cross section (n=3) and each velocity (n=3), for a total of 9 data points.

canopy interface. Within the canopy, Da numbers were higher than in the open channel ($\mathrm{Da_{vc}} > \mathrm{Da_{oc}}$) for all $\mathrm{U_{nom}}$ (Figure 5e) demonstrating that in the canopy $\mathrm{NO_3}^-\mathrm{N}$ removal was more limited by the transport of resources (DOC , $\mathrm{NO_3}^-\mathrm{N}$) to reactive surfaces (dowel biofilms) and less limited by the rate $\mathrm{NO_3}^-\mathrm{N}$ was removed by microbial processes on those surfaces. Conversely, the $\mathrm{Da_{oc}}$ numbers were lower, less variable, and generally increased with $\mathrm{U_{nom}}$ indicating that $\mathrm{NO_3}^-\mathrm{N}$ removal was even more reaction limited and less subject to local controls than in the VC. In other words, $\mathrm{NO_3}^-\mathrm{N}$ removal in the open channel was likely more limited by fewer reactive surfaces in contact with the flowing water than the canopy, while the canopy was more limited by transport of reaction limiting resources, in this case $\mathrm{NO_3}^-\mathrm{N}$, than the open channel. These zonal differences in dominant hydro-biogeochemical controls agrees with findings from other significant interfacial hot spots, such as SWIs (Frei et al., 2012; O'Connor & Hondzo, 2008; Stegen et al., 2022).

The increasing-to-plateau relationship for Da_{oc} with U_{nom} (Figure 5e) suggests that the reactive surfaces of the OC were sensitive to the higher turbulence at the interface (Figure 4f). The observed initial increase in Da_{oc} numbers with increasing U_{nom} suggest that open channel mass transfer limitations decreased initially, until at high U_{nom} the biofilms capacity to remove NO_3^-N or withstand the flow conditions was exceeded (Larned et al., 2004; Thomas & Cornelisen, 2003). Hydrodynamic profiles support this reasoning by showing that the canopy interface was subject to greater stress from mixing, especially at higher U_{nom} , as peak TKE occurs at canopy interface and maximum TKE increased with U_{nom} (Figures 4d and 4f). These results substantiate the mechanisms discussed in 4.2 (scour and expansive oxic zones), and that trade-offs in hydro-biogeochemical conditions are crucial components of nutrient transformations at critical hydro-biogeochemical interfaces (i.e., O'Connor & Hondzo, 2008; Harvey et al., 2019).

The relationships between dimensionless zonal Da numbers and Re_{oc} further corroborate that NO₃⁻N removal within the two zones, VC and OC, are subject to different controls. Here, we observed that Da_{oc} exhibited significant relationships with Re_{oc} ($R^2 = 0.74$; Figure 10a). The positive Da-Re relationship suggests that NO₃⁻N removal in the OC is not as limited by local flow conditions or transport of NO₃⁻N. The positive relationship between $\langle k_{rN} \rangle_{oc}$ and w_{oc} similarly suggests that the mixing in the open channel, just outside the interface, induces removal ($R^2 = 0.73$; Figure 10c). The VC however, exhibits a threshold as Re_{oc} increases, suggesting that the canopy initially benefits from increasing flow in the OC until negative impacts of flow on the canopy, such as scour, occur. Low Re thresholds have been

observed for periphyton assemblages, such as the biofilms observed on canopy dowels, suggesting the biofilms are only relevant for N removal under low flow conditions before they are physically damaged or removed (e.g., Dodds & Biggs, 2002). Furthermore, $\langle k_{rN} \rangle_{vc}$ exhibits no significant relationships with hydrodynamics, within or outside the canopy, suggesting alternate, likely biogeochemical, controls (Figure S2 in Supporting Information S1).

The dimensionless Da-Re framework could be useful for identifying and leveraging hydro-biogeochemical controls to improve NO_3^-N removal across scales (e.g., Pinay et al., 2015) with future work. Re_{oc} can be calculated through relatively easy to measure or attainable variables (i.e., velocity, water depth, and viscosity; Equation 6). However, future work should aim to more efficiently estimate canopy-induced rates of mass transport at reach or larger scales. In order to bridge understanding between hydrodynamics and biogeochemistry for N removal in vegetated surface water systems, we defined rates of mass transport based on turbulent energy generation and dissipation (TKE and ϵ) in open channel or vegetated flows. This approach is data intensive and

WATERMAN AND HANSEN 17 of 25

not easily transferable to field scales. Defining transport times from residence time distributions or longitudinal dispersion coefficients (Nifong & Taylor, 2021; Sharp et al., 2021), similar to what is already employed in other environments (i.e., hyporheic zone; Azizian et al., 2017; Ocampo et al., 2006), would be an ideal approach for assessing controls on N removal through vegetation at field to reach scales. Moreover, Da-Re metrics need to be measured and relationships validated in real vegetated aquatic systems, and under more variable flow and environmental conditions, to develop a quantitative framework that could be leveraged to enhance N removal.

4.4. Implications for Vegetation Management

Even within our controlled setting, we observed convoluted effects of both hydrodynamics and biogeochemistry with a canopy of model vegetation that both positively and negatively influenced N removal. Such results lead us to stress the importance of understanding how best to manage vegetation as a solution to degraded water quality. We only explored the effects of one density, canopy length and rigidity here, however further research on how live vegetation, which introduces additional hydrological and biogeochemical variability, influences N removal is crucial to address so that land managers and engineers can make informed, science-based decisions on designing ecosystems to mitigate excess N.

Hydrodynamics near vegetation are dependent on the physical properties of the vegetation canopy itself (Caroppi et al., 2019; Nepf, 1999). As such, selecting or managing aspects such as canopy or patch lengths, composition, density, vegetation rigidity (or flexibility) are ideal management strategies to enhance N removal from flowing water ways (Bal et al., 2013; Cornacchia et al., 2019). For example, the hydrodynamic flow profiles demonstrate that specific locations along the canopy can serve as locations of enhanced N removal (Figures 4a-4c). Profiles of streamwise and lateral velocity $(\overline{u}/U_{nom},\overline{v}/U_{nom},$ respectively) show the flowing water that encountered the canopy initially was routed out (at XS1), while flows along the canopy length (to XS3) were routed toward the interface and into the canopy. The vertical direction (\overline{w}/U_{nom}) was the most complex along each XS, with water routed down initially at XS1, then routed up at XS2 and XS3. Regardless of XS and U_{nom} , there was always a consistent positive inflection point at the interface, indicating that water was being routed up and into the canopy. Together, these profiles suggest that water rich in organic C is pulled out of the canopy initially, mixed with oxic, NO₃⁻N rich water in or near the open channel sediments at XS1, until being routed back up and into the interface/ canopy at XS2 and XS3. Indeed, NO₃⁻N removal rates were noticeably higher at XS2 for intermediate and XS3 for high flows, respectively (Figure 6b). This implicates the canopy interface (after the initial entrance effects) as a location of enhanced NO₃⁻N removal and suggest that canopy length is an important variable that can influence N removal efficiency of vegetated canopies.

As another example, real vegetation creates significantly wider exchange zones with the open channel (here, w_{ml}) compared to model rigid cylinders commonly used in hydrodynamic studies (i.e., Caroppi et al., 2021) that could have outsized effects on N removal. For example, the open channel NO₃⁻N removal rates were significantly dependent on the open channel portion of the mixing zone, w_{oc} (Figure 10c; $R^2 = 0.73$). The enhanced mixing, and thus heightened N removal, of this zone occurs because of the lowered velocity, increased production and dissipation of energy and rates of mass transport across the canopy interface. Although the mixing zone width is well studied, it is complex and not easily constrained (e.g., Caroppi et al., 2021; Truong & Uijttewaal, 2019; White & Nepf, 2007). Here, we observed that w_{oc} is negatively related to canopy flow conditions (U_{vc} and Re_{vc} ; $R^2 > 0.43$; Figure S2 in Supporting Information S1). These relationships might be useful for scaling and predicting this key driver of NO_3^-N removal at larger scales, as canopy mean velocity (U) and Re numbers are relatively easy to measure or model (e.g., White & Nepf, 2008).

Optimizing N removal in real landscapes is complicated by variable flow conditions and natural vegetation. The results presented in this study suggest slow to moderate flow conditions are best for N removal, but these are not the conditions that often have the highest N loads, as event hydrology is a dominant driver of N transport from many, particularly agricultural, landscapes (Bolade & Hansen, 2023). In already highly modified systems, such as agricultural ditches or treatment wetlands, low to moderate flow conditions could be sustained by modifying hydraulic design or management. These systems are often managed to remove water as quickly as possible, for example, by channel straightening or removing vegetation, yet if water quality is also a valued ecosystem service, then management could be adjusted to optimize N removal (Dollinger et al., 2015; Kalinowska et al., 2023; Rudi et al., 2020; Soana, Gavioli, et al., 2018; Soana et al., 2019; Tamburini et al., 2020). Conversely, natural systems are much more variable in terms of flow and vegetation, requiring careful placement of landscape features such as

WATERMAN AND HANSEN 18 of 25



riparian or riverine wetlands to slow down high flows and provide C for optimal N removal (Hansen et al., 2016, 2018). In many regions, ongoing changes in land use and climate have increased the intensity and peak flows in aquatic systems which complicates effective land management (Milly et al., 2005; Wang & Hejazi, 2011). As such, we recommend future studies to investigate how canopies of real rigid emergent vegetation impact mixing and mass transfer under a wider, more variable, range of flow and N load conditions, coupled with in situ observations of N removal rates, to see how the mechanisms identified here hold.

Our study investigated effects of artificial rigid vegetation, intentionally removing biological complexities from our experimental design to focus on hydrodynamic-driven mechanisms of mass transfer on NO₃⁻N removal. As such, our findings are more relevant to dormant or senesced vegetation, similar to Soana, Gavioli, et al. (2018) who investigated flow through dead stems of reeds (Phragmites australis). Live aquatic vegetation will complicate N cycling, via N assimilation, C leaching, and rhizosphere processes that influences DO and redox dynamics (Philippot et al., 2013; Sharp et al., 2021). C and N ratios of organic matter (OM) from real aquatic vegetation are highly species and environmentally dependent (Hume et al., 2002; Walton et al., 2020; Wang et al., 2019), thus for management it is crucial to identify plants and conditions that provide ideal C concentrations and types, yet minimally leach N. Previous research on rigid aquatic vegetation commonly found in agricultural ditches or treatment wetlands, such as reeds (Phragmites species) and cattails (Typha species), show that these highly productive species have high and bioavailable C and low N content (Hume et al., 2002; Wang et al., 2019; Zhang et al., 2014), suggesting these species are ideal starting candidates to optimize resource controls for N removal in aquatic ecosystems. However, vegetation selection for ecosystem services such as NO₃⁻N removal need to be studied in context of other ecosystem (dis)services, as some vegetation species are invasive (Bansal et al., 2019; Sharp et al., 2021) and may increase greenhouse gas emissions (Burgin et al., 2013; Kasak et al., 2020; Reay et al., 2003).

Our results expose uncertainties that still remain in terms of managing vegetation (e.g., mowing or harvesting) for water quality improvements (Jabłońska et al., 2021; Soana, Gavioli, et al., 2018; Soana et al., 2019; Tamburini et al., 2020). The complicated effects of vegetative canopies, or their removal, on N processing in aquatic environments can be observed by the stark differences between CN relationships and TDN concentrations between the canopy and control experiments (Figure 8 and Figure S1 in Supporting Information S1). These results, specifically the lack of DOC variability with NO₃⁻N (Figure 8), and initial increases in NO₃⁻N at low velocity and overall increases TDN (Figure S1 in Supporting Information S1), suggest that the removal of the canopy for the control experiments introduced sediment or pore water bound OM that inhibited NO₃-N removal for the control experiments (Figure 9). Inputs of labile (i.e., glucose) and terrestrial OM (i.e., crushed leaves) into aquatic systems both can increase microbial processing, specifically bacterial mineralization (de Moura et al., 2022; Mineau et al., 2016). Enhanced microbial activity from OM mineralization would drive DOC concentrations down, as observed (Figure 7b), while not necessarily resulting in high rates of NO₃¬N removal (Figure 9). Furthermore, OM also contains organic N that can undergo mineralization and the subsequent stepwise oxidation of inorganic N (NH₄ to NO_x to NO₃⁻N) could have muted or lagged NO₃⁻N removal (Figure S1 in Supporting Information S1). Thus, we conject that as stored OM was exposed and mixed through the mesocosm, organic C and N were mineralized as the more labile DOC was utilized, which introduced various N species and removed energy sources that together negatively impacted NO₃-N removal for the control experiments. This suggests that harvesting vegetation should minimize disturbance of the soil and subsequent introduction of stored OM, and well-timed, to balance detritus accumulation for reactive surfaces versus potential organic N leaching to mitigate this kind of response (Jabłońska et al., 2021; Soana, Gavioli, et al., 2018). In general, such responses underscore the complex nature of N and C processing in real aquatic ecosystems (i.e., Ahamed et al., 2023; Barnes et al., 2012; Czuba et al., 2018; Kunza & Hall, 2014) and the importance of understanding how aquatic ecosystems will respond to new and/or changing C and N inputs prior to widespread implementation of vegetation as a management strategy.

5. Conclusions

To our knowledge, this study is the first to mechanistically investigate the combined effects of fluid flow conditions (specifically U_{nom} and rates of mass transport) and rigid, emergent vegetative canopy presence on NO_3^- N removal. Our findings demonstrate that interfaces of canopies of emergent vegetation in flowing water ways can be locations of enhanced NO_3^- N removal on the landscape (i.e., a hotspot) due to convergence and sustaining of microbial reaction limiting resources (DOC and NO_3^- N) (Figures 7 and 8)

WATERMAN AND HANSEN 19 of 25

19447973, 2024, 8, Downloaded from

nline library.wiley.com/doi/10.1029/2023WR036995 by Amy Hansen , Wiley Online Library on [30/07/2024]. See the Terms and Conditions (https://onlinelibrary.wiley.com/terms

and-conditions) on Wiley Online Library for rules of use; OA articles are governed by the applicable Crea

and heightened, complex mixing at and along the canopy interface (Figure 4). Different trends with zonal Da and open channel Re numbers show that NO₃⁻ N removal within the canopy and open channel zones are subject to different controls (Figures 5 and 6). The relationships between open channel NO₃⁻N removal rates with open channel hydrodynamic metrics (mixing zone width and Re) at this interface can guide further studies on management practices to optimize emergent vegetative canopies to improve N removal in natural environments (Figure 10). The results of this study increase our understanding of drivers of NO₃⁻N removal at the interface between flowing waters of open channels and canopies of rigid vegetation and provide significant relationships for researchers and land managers to consider when investigating and implementing vegetation as a solution to excess N loading.

Appendix A

 Table A1

 Table Containing Information on Canopy Details and Dimensions

Parameter	Value	Units	Definition			
A	16.22	m^{-1}	Average solid frontal area per unit volume			
d	0.006	m	Cylinder diameter			
N	2555	nm^{-2}	Density of cylinders (number cylinders/unit area)			
Φ	0.081	m	Solid volume fraction			
S	0.013	m	Distance between cylinders			
В	0.46	m	Flume width			
b	0.23	m	Vegetated canopy width			
H	0.23	m	Mean water depth			
L_c	1.80	m	Length of canopy			
L_f	5.20	m	Length of flume			

Note. The canopy was designed to emulate canopies of real aquatic vegetation and to be consistent other hydrodynamic studies.

Table A2 *Manuscript Variables, Units, and Definitions Relating to Hydrodynamics and Dimensionless Numbers*

Parameter	Units	Definition
\overline{U}	cms ⁻¹	Nominal velocity, temporally averaged
$\langle \overline{U} angle$	cms^{-1}	Velocity, temporally and spatially averaged
$\overline{u'v'}$	cms^{-1}	Reynold's stresses
Re	dim.	Reynold's number
W_{ml}	cm	Width of mixing zone
W_{oc}	cm	Portion of mixing width that is in open channel
W_{vc}	cm	Shear extent into the canopy
$\langle TKE \rangle$	$\mathrm{cm}^2\mathrm{s}^{-2}$	Average turbulent kinetic energy, spatially averaged
$\langle arepsilon angle$	$\mathrm{cm}^2\mathrm{s}^{-3}$	Average turbulent dissipation, spatially averaged
$\langle k_m \rangle$	cms^{-1}	Mass transport rate
$\langle \kappa_{rN} angle$	$1s^{-1}$	First order reaction rate for N removal
Da	dim.	Damköhler number

WATERMAN AND HANSEN 20 of 25

1944/973, 2024, 8, Downloaded from https://agupubs.onlinelibrary.wiley.com/doi/10.1029/2023WR036995 by Amy Hansen , Wiley Online Library on [30.07/2024]. See the Terms and Conditions (https://onlinelibrary.wiley.com/terms

and-conditions) on Wiley Online Library for rules of use; OA articles are governed by the applicable Creati

 Table A3

 Hydrodynamic Results by Velocity (U_{nom}) and Cross Section (XS)

		2 (nom		, ,					
	3 cm/s (Low)			6 cm/s (Intermediate)			9 cm/s (High)		
Parameter (units)	XS1	XS2	XS3	XS1	XS2	XS3	XS1	XS2	XS3
U (cms ⁻¹)	2.59	2.75	3.55	4.92	5.81	6.13	7.39	8.90	8.94
$\langle \overline{\rm U} \rangle_{\rm oc} \ ({\rm cm s^{-1}})$	6.88	6.74	6.89	13.7	15.2	15.5	18.2	20.2	19.7
$\langle \overline{\mathrm{U}} \rangle_{\mathrm{vc}} \; (\mathrm{cms}^{-1})$	0.220	0.020	0.050	0.430	0.243	0.194	1.42	1.36	0.304
$\langle \overline{\mathrm{U}} \rangle_{\mathrm{ml}} \; (\mathrm{cms}^{-1})$	2.53	2.54	3.91	4.95	6.25	6.28	6.03	7.56	9.08
Re oc	1.76E4	1.73E4	1.77E4	3.52E4	3.90E4	3.96E4	4.66E4	5.16E4	5.03E4
Re vc	15.73	1.30	3.85	30.6	17.3	13.8	101	96.6	21.7
Re ml	6.47E3	6.49E3	1.00E4	1.27E4	1.32E4	1.61E4	1.54E4	1.94E4	2.33E4
w _{ml} (cm)	9.20	12.6	12.4	11.3	18.1	22.7	9.10	10.7	15.0
w _{oc} (cm)	9.20	10.5	11.1	11.3	13.2	13.7	7.50	7.95	9.17
w _p (cm)	-0.82	2.06	1.34	-1.27	4.88	8.99	1.60	2.75	5.83
$\langle \text{TKE} \rangle_{\text{oc}} (\text{cm}^2 \text{s}^{-2})$	0.648	1.89	1.56	4.11	5.51	8.58	2.08	7.22	13.1
$\langle \text{TKE} \rangle_{\text{vc}} (\text{cm}^2 \text{s}^{-2})$	0.340	0.147	0.759	0.339	0.958	1.43	0.617	2.07	4.74
$\langle \epsilon \rangle_{\rm oc} ({\rm cm}^2 {\rm s}^{-3})$	0.072	0.331	0.250	1.24	1.67	3.12	0.467	2.58	5.60
$\langle \epsilon \rangle_{\rm vc} \ ({\rm cm}^2 {\rm s}^{-3})$	1.02	0.265	3.82	1.09	5.37	9.45	2.16	6.05	63.4

 $\textbf{Table A4} \\ Water \textit{Chemistry Results (Means and Standard Deviations) by Nominal Velocity (U_{nom}: Low, Intermediate, and High), Zone (OC and VC) and No Canopy Control (NC) } \\$

Parameter (units)	3 cm/s (Low)			6 cm/s (Intermediate)			9 cm/s (High)		
	OC	VC	NC	OC	VC	NC	OC	VC	NC
⟨ <i>DO</i> ⟩ (%)	84.9	71.2	71.6	90.5	83.6	73.	96.1	93.6	83.8
	6.24	14.5	10.5	7.66	10.5	20.7	4.79	5.08	11.0
$\langle C/C_{max} \rangle$	0.406	0.504	0.631	0.452	0.440	0.636	0.608	0.643	0.590
	0.014	0.184	0.264	0.171	0.095	0.284	0.025	0.095	0.251
$\langle N/N_{max} \rangle$	0.852	0.823	0.789	0.724	0.715	0.690	0.787	0.770	0.854
	0.061	0.081	0.041	0.099	0.090	0.070	0.086	0.079	0.021
$\langle \mathit{CN}_{\mathit{max}} \rangle$	0.478	0.620	0.787	0.612	0.613	0.894	0.784	0.843	0.690
	0.028	0.246	0.289	0.155	0.088	0.310	0.112	0.142	0.292
$\langle \text{Temp} \rangle (C)$	26.8	26.8	30.8	25.6	25.6	26.2	31.0	30.7	23.0
	0.367	0.358	2.81	0.965	1.00	3.17	3.97	4.25	4.24
$\langle \kappa_{rN} \rangle (s^{-1})$	4.69E-6	5.41E-6	1.78E-6	8.71E-6	6.66E-6	4.46E-6	4.32E-6	3.72E-6	4.45E-7
	4.12E-7	1.65E-6		1.14E-6	1.50E-6		5.72E-7	4.70E-6	
$\langle k_{rN_exp} \rangle \ (s^{-1})$	5.51E-6	6.82E-6	2.83E-6	9.15E-6	6.99E-6	4.92E-6	6.91E-6	5.95E-6	3.78E-7
·	4.76E-7	1.91E-6		1.20E-6	1.57E-7		9.15E-7	7.52E-6	

WATERMAN AND HANSEN 21 of 25

19447973, 2024, 8, Downloaded from https:

onlinelibrary.wiley.com/doi/10.1029/2023WR036995 by Amy

Data Availability Statement

Data sets for this research are available and can be found here: Waterman and Hansen (2024). Experimental data sets used to investigate hydro-biogeochemical controls on nitrate removal at the interface of flowing water and artificial emergent vegetation. https://doi.org/10.17605/OSF.IO/ZN29W.

Acknowledgments

This research was funded by the National Science Foundation (NSF) through a NSF CAREER grant (EAR-2339873) and through a University of Kansas New Faculty General Research Fund Award. both to A.T.H. The authors are grateful to EcoFluids undergraduate students who have contributed significant time and effort in the both the fluids and chemistry labs to this work, specifically Allison Dobie, Tessa Rothwell, Joseph Hawker, Hannah Minn and Joey Craft. Additional thanks to Dr. Amy Burgin for helpful discussions on N biogeochemistry at the onset of experiments. Finally, the authors thank the editor, the associate editor, and two anonymous reviewers for their time and constructive comments that improved the

References

- Ahamed, F., You, Y., Burgin, A., Stegen, J. C., Scheibe, T. D., & Song, H.-S. (2023). Exploring the determinants of organic matter bioavailability through substrate-explicit thermodynamic modeling. Frontiers in Water, 5. https://doi.org/10.3389/frwa.2023.1169701
- Arnon, S., Peterson, C. G., Gray, K. A., & Packman, A. I. (2007). Influence of flow conditions and system geometry on nitrate use by benthic biofilms: Implications for nutrient mitigation. *Environmental Science & Technology*, 41(23), 8142–8148. https://doi.org/10.1021/es0710048
- Azizian, M., Boano, F., Cook, P. L. M., Detwiler, R. L., Rippy, M. A., & Grant, S. B. (2017). Ambient groundwater flow diminishes nitrate processing in the hyporheic zone of streams. *Water Resources Research*, 53(5), 3941–3967. https://doi.org/10.1002/2016WR020048
- Bachand, P. A. M., & Horne, A. J. (1999). Denitrification in constructed free-water surface wetlands: II. Effects of vegetation and temperature. *Ecological Engineering*, 14(1), 17–32. https://doi.org/10.1016/S0925-8574(99)00017-8
- Bal, K. D., Brion, N., Woulé-Ebongué, V., Schoelynck, J., Jooste, A., Barrón, C., et al. (2013). Influence of hydraulics on the uptake of ammonium by two freshwater plants. Freshwater Biology, 58(12), 2452–2463. https://doi.org/10.1111/fwb.12222
- Bansal, S., Lishawa, S. C., Newman, S., Tangen, B. A., Wilcox, D., Albert, D., et al. (2019). Typha (Cattail) invasion in North American wetlands: Biology, regional problems, impacts, ecosystem services, and management. *Wetlands*, 39(4), 645–684. https://doi.org/10.1007/s13157-019-01174-7
- Barnes, R. T., Smith, R. L., & Aiken, G. R. (2012). Linkages between denitrification and dissolved organic matter quality, Boulder Creek watershed, Colorado. *Journal of Geophysical Research: Biogeosciences*, 117(G1). https://doi.org/10.1029/2011JG001749
- Bastviken, S. K., Weisner, S. E. B., Thiere, G., Svensson, J. M., Ehde, P. M., & Tonderski, K. S. (2009). Effects of vegetation and hydraulic load on seasonal nitrate removal in treatment wetlands. *Ecological Engineering*, 35(5), 946–952. https://doi.org/10.1016/j.ecoleng.2009.01.001
- Birgand, F., Skaggs, R. W., Chescheir, G. M., & Gilliam, J. W. (2007). Nitrogen removal in streams of agricultural catchments—A literature review. Critical Reviews in Environmental Science and Technology, 37(5), 381–487. https://doi.org/10.1080/10643380600966426
- Böhlke, J. K., Antweiler, R. C., Harvey, J. W., Laursen, A. E., Smith, L. K., Smith, R. L., & Voytek, M. A. (2009). Multi-scale measurements and modeling of denitrification in streams with varying flow and nitrate concentration in the upper Mississippi River basin, USA. *Biogeochemistry*, 93(1–2), 117–141. https://doi.org/10.1007/s10533-008-9282-8
- Bolade, O., & Hansen, A. T. (2023). Inferring drivers of nitrate and sediment event dynamics from hysteresis metrics for two large agricultural watersheds. *Hydrological Processes*, 37(9), e14969. https://doi.org/10.1002/hyp.14969
- Brune, A., Frenzel, P., & Cypionka, H. (2000). Life at the oxic–anoxic interface: Microbial activities and adaptations. FEMS Microbiology Reviews, 24(5), 691–710. https://doi.org/10.1111/j.1574-6976.2000.tb00567.x
- Burgin, A. J., Lazar, J. G., Groffman, P. M., Gold, A. J., & Kellogg, D. Q. (2013). Balancing nitrogen retention ecosystem services and greenhouse gas disservices at the landscape scale. *Ecological Engineering*, 56, 26–35. https://doi.org/10.1016/j.ecoleng.2012.05.003
- Caroppi, G., Västilä, K., Gualtieri, P., Järvelä, J., Giugni, M., & Rowiński, P. M. (2021). Comparison of flexible and rigid vegetation induced shear layers in partly vegetated channels. Water Resources Research, 57(3), e2020WR028243. https://doi.org/10.1029/2020WR028243
- Caroppi, G., Västilä, K., Gualtieri, P., Järvelä, J., Rowiński, P. M., & Giugni, M. (2019). Turbulence at water-vegetation interface in open channel flow: Experiments with natural-like plants. Advances in Water Resources, 127, 180–191. https://doi.org/10.1016/j.advwatres.2019.03.013
- Castaldelli, G., Aschonitis, V., Vincenzi, F., Fano, E. A., & Soana, E. (2018). The effect of water velocity on nitrate removal in vegetated waterways. *Journal of Environmental Management*, 215, 230–238. https://doi.org/10.1016/j.jenvman.2018.03.071
- Castaldelli, G., Soana, E., Racchetti, E., Vincenzi, F., Fano, E. A., & Bartoli, M. (2015). Vegetated canals mitigate nitrogen surplus in agricultural watersheds. *Agriculture, Ecosystems & Environment*, 212, 253–262. https://doi.org/10.1016/j.agee.2015.07.009
- watersneas. Agriculture, Ecosystems & Environment, 212, 255–262. https://doi.org/10.1016/j.agee.2015.07.009

 Chen, R., Deng, M., He, X., & Hou, J. (2017). Enhancing nitrate removal from freshwater pond by regulating carbon/nitrogen ratio. Frontiers in
- Microbiology, 8. https://doi.org/10.3389/fmicb.2017.01712
 Cheng, F. Y., & Basu, N. B. (2017). Biogeochemical hotspots: Role of small water bodies in landscape nutrient processing. Water Resources
- Research, 53(6), 5038–5056. https://doi.org/10.1002/2016WR020102
 Conley, D. J., Paerl, H. W., Howarth, R. W., Boesch, D. F., Seitzinger, S. P., Havens, K. E., et al. (2009). Controlling eutrophication: Nitrogen and
- phosphorus. Science, 323(5917), 1014–1015. https://doi.org/10.1126/science.1167755

 Cornacchia, L., Licci, S., Nepf, H., Folkard, A., van der Wal, D., van de Koppel, J., et al. (2019). Turbulence-mediated facilitation of resource
- uptake in patchy stream macrophytes. *Limnology & Oceanography*, 64(2), 714–727. https://doi.org/10.1002/ino.11070

 Covino, T. (2017). Hydrologic connectivity as a framework for understanding biogeochemical flux through watersheds and along fluvial networks. *Geomorphology*, 277, 133–144. https://doi.org/10.1016/j.geomorph.2016.09.030
- Czuba, J. A., Hansen, A. T., Foufoula-Georgiou, E., & Finlay, J. C. (2018). Contextualizing wetlands within a river network to assess nitrate
- removal and inform watershed management. Water Resources Research, 54(2), 1312–1337. https://doi.org/10.1002/2017WR021859 de Moura, C. G. B., Rocha, E., de Attayde, J. L., Noyma, N., de Oliveira Vidal, L., Fonseca, L. M., et al. (2022). Fresh terrestrial detritus fuels both
- de Moura, C. G. B., Rocha, E., de Attayde, J. L., Noyma, N., de Oliveira Vidal, L., Fonseca, L. M., et al. (2022). Fresh terrestrial detritus fuels both heterotrophic and autotrophic activities in the planktonic food web of a tropical reservoir: A mesocosm study. *Hydrobiologia*, 849(17), 3931–3946. https://doi.org/10.1007/s10750-021-04754-z
- Dodds, W. K., & Biggs, J. F. (2002). Water velocity attenuation by stream periphyton and macrophytes in relation to growth form and architecture. Journal of the North American Benthological Society, 21(1), 2–15. https://doi.org/10.2307/1468295
- Dollinger, J., Dag`es, C., Bailly, J. S., Lagacherie, P., & Voltz, M. (2015). Managing ditches for agroecological engineering of landscape. A review. Agronomy for Sustainable Development, 35(3), 999–1020. https://doi.org/10.1007/s13593-015-0301-6
- Frei, S., Knorr, K. H., Peiffer, S., & Fleckenstein, J. H. (2012). Surface micro-topography causes hot spots of biogeochemical activity in wetland systems: A virtual modeling experiment: Micro-topography and hot spot formation. *Journal of Geophysical Research*, 117(G4). https://doi.org/ 10.1029/2012JG002012
- Ghisalberti, M. (2009). Obstructed shear flows: Similarities across systems and scales. *Journal of 964 Fluid Mechanics*, 641, 51–61. https://doi.org/10.1017/S0022112009992175
- Ghisalberti, M., & Nepf, H. (2005). Mass transport in vegetated shear flows. Environmental Fluid Mechanics, 5(6), 527–551. https://doi.org/10. 1007/s10652-005-0419-1

WATERMAN AND HANSEN 22 of 25



Water Resources Research

- 10.1029/2023WR036995
- Ghisalberti, M., & Nepf, H. M. (2002). Mixing layers and coherent structures in vegetated aquatic flows. *Journal of Geophysical Research: Oceans*, 107(C2), 3-1-3-11. https://doi.org/10.1029/2001JC000871
- Ghisalberti, M., & Nepf, H. M. (2004). The limited growth of vegetated shear layers. Water Resources Research, 40(7). https://doi.org/10.1029/2003WR002776
- Glenn, E., Thompson, T., Frye, R., Riley, J., & Baumgartner, D. (1995). Effects of salinity on growth and evapotranspiration of Typha domingensis Pers. *Aquatic Botany*, 52(1), 75–91. https://doi.org/10.1016/0304-3770(95)00492-i
- Goldman, E., & Jacobs, R. (1961). Determination of nitrates by ultraviolet absorption. *Journal (American Water Works Association)*, 53(2), 187–191. https://doi.org/10.1002/j.1551-8833.1961.tb00651.x
- Grant, S. B., Gomez-Velez, J. D., & Ghisalberti, M. (2018). Modeling the effects of turbulence on hyporheic exchange and local-to-global nutrient processing in streams. Water Resources Research, 54(9), 5883–5889. https://doi.org/10.1029/2018WR023078
- Gruber, N., & Galloway, J. N. (2008). An Earth-system perspective of the global nitrogen cycle. *Nature*, 451(7176), 293–296. Article 7176. https://doi.org/10.1038/nature06592
- Gu, C., Hornberger, G. M., Mills, A. L., Herman, J. S., & Flewelling, S. A. (2007). Nitrate reduction in streambed sediments: Effects of flow and biogeochemical kinetics. Water Resources Research, 43(12). https://doi.org/10.1029/2007WR006027
- Hansen, A., Dolph, C., Foufoula-Georgiou, E., & Finlay, J. (2018). Contribution of wetlands to nitrate removal at the watershed scale. *Nature Geoscience*, 11(2), 127–132. https://doi.org/10.1038/s41561-017-0056-6
- Hansen, A. T., Dolph, C. L., & Finlay, J. C. (2016). Do wetlands enhance downstream denitrification in agricultural landscapes? *Ecosphere*, 7(10), e01516. https://doi.org/10.1002/ecs2.1516
- Harvey, J., Gomez-Velez, J., Schmadel, N., Scott, D., Boyer, E., Alexander, R., et al. (2019). How hydrologic connectivity regulates water quality in river corridors. JAWRA Journal of the American Water Resources Association, 55(2), 369–381. https://doi.org/10.1111/1752-1688.12691
- Holland, J. F., Martin, J. F., Granata, T., Bouchard, V., Quigley, M., & Brown, L. (2004). Effects of wetland depth and flow rate on residence time distribution characteristics. *Ecological Engineering*, 23(3), 189–203. https://doi.org/10.1016/j.ecoleng.2004.09.003
- Hume, N. P., Fleming, M. S., & Horne, A. J. (2002). Denitrification potential and carbon quality of four aquatic plants in wetland microcosms. *Soil Science Society of America Journal*, 66(5), 1706–1712. https://doi.org/10.2136/sssaj2002.1706
- Science Society of America Journal, 60(3), 1706–1712. https://doi.org/10.2136/sssaj.2002.1706

 Ikeda, S., & Kanazawa, M. (1996). Three-dimensional organized vortices above flexible water plants. *Journal of Hydraulic Engineering*, 122(11), 634–640. https://doi.org/10.1061/(ASCE)0733-9429(1996)122:11(634)
- Jabłońska, E., Winkowska, M., Wiśniewska, M., Geurts, J., Zak, D., & Kotowski, W. (2021). Impact of vegetation harvesting on nutrient removal and plant biomass quality in wetland buffer zones. *Hydrobiologia*, 848(14), 3273–3289. https://doi.org/10.1007/s10750-020-04256-4
- Johnson, L. T., Royer, T. V., Edgerton, J. M., & Leff, L. G. (2012). Manipulation of the dissolved organic carbon pool in an agricultural stream: Responses in microbial community structure, denitrification, and assimilatory nitrogen uptake. *Ecosystems*, 15(6), 1027–1038. https://doi.org/ 10.1007/s10021-012-9563-x
- Kadlec, R. H., & Wallace, S. D. (2009). Treatment wetlands (2nd ed.). CRC Press.
- Kalinowska, M. B., Västilä, K., Nones, M., Kiczko, A., Karamuz, E., Brandyk, A., et al. (2023). Influence of vegetation maintenance on flow and mixing: Case study comparing fully cut with high-coverage conditions. *Hydrology and Earth System Sciences*, 27(4), 953–968. https://doi.org/10.5194/hess-27-953-2023
- Kasak, K., Valach, A. C., Rey-Sanchez, C., Kill, K., Shortt, R., Liu, J., et al. (2020). Experimental harvesting of wetland plants to evaluate trade-offs between reducing methane emissions and removing nutrients accumulated to the biomass in constructed wetlands. Science of the Total Environment, 715, 136960, https://doi.org/10.1016/j.scitoteny.2020.136960
- $Knowles, R. \ (1982). \ Denitrification. \ \textit{Microbiological Reviews}, 46 (1), 43-70. \ https://doi.org/10.1128/mr.46.1.43-70.1982$
- Kreiling, R. M., Richardson, W. B., Cavanaugh, J. C., & Bartsch, L. A. (2010). Summer nitrate uptake and denitrification in an upper Mississippi River backwater lake: The role of rooted aquatic vegetation. *Biogeochemistry*, 104(1–3), 309–324. https://doi.org/10.1007/s10533-010-9503-9
- Kunza, L. A., & Hall, R. O. (2014). Nitrogen fixation can exceed inorganic nitrogen uptake fluxes in oligotrophic streams. *Biogeochemistry*, 121(3), 537–549. https://doi.org/10.1007/s10533-014-0021-z
- Larned, S. T., Nikora, V. I., & Biggs, B. J. F. (2004). Mass-transfer-limited nitrogen and phosphorus uptake by stream periphyton: A conceptual model and experimental evidence. *Limnology & Oceanography*, 49(6), 1992–2000. https://doi.org/10.4319/lo.2004.49.6.1992
- Levi, P. S., Riis, T., Alnøe, A. B., Peipoch, M., Maetzke, K., Bruus, C., & Baattrup-Pedersen, A. (2015). Macrophyte complexity controls nutrient untake in lowland streams. *Ecosystems*, 18(5), 914–931. https://doi.org/10.1007/s10021-015-9872-v
- uptake in lowland streams. *Ecosystems*, 18(5), 914–931. https://doi.org/10.1007/s10021-015-9872-y Lin, Y.-F., Jing, S.-R., Wang, T.-W., & Lee, D.-Y. (2002). Effects of macrophytes and external carbon sources on nitrate removal from
- groundwater in constructed wetlands. Environmental Pollution, 119(3), 413–420. https://doi.org/10.1016/S0269-7491(01)00299-8
 Liu, M. (柳梦阳), Huai, W. (槐文信), Ji, B. (季斌), & Han, P. (韩鵬). (2021). Numerical study on the drag characteristics of rigid submerged vegetation patches. Physics of Fluids, 33(8), 085123. https://doi.org/10.1063/5.0060601
- Longhi, D., Bartoli, M., & Viaroli, P. (2008). Decomposition of four macrophytes in wetland sediments: Organic matter and nutrient decay and associated benthic processes. Aquatic Botany, 89(3), 303–310. https://doi.org/10.1016/j.aquabot.2008.03.004
- Marion, A., Nikora, V., Puijalon, S., Bouma, T., Koll, K., Ballio, F., et al. (2014). Aquatic interfaces: A hydrodynamic and ecological perspective. Journal of Hydraulic Research, 52(6), 744–758. https://doi.org/10.1080/00221686.2014.968887
- Meftah, M. B., De Serio, F., & Mossa, M. (2014). Hydrodynamic behavior in the outer shear layer of partly obstructed open channels. *Physics of Fluids*, 26(6), 065102. https://doi.org/10.1063/1.4881425
- Milly, P., Dunne, K., & Vecchia, A. (2005). Global pattern of trends in streamflow and water availability in a changing climate. *Nature*, 438(7066), 347–350. https://doi.org/10.1038/nature04312
- Mineau, M. M., Wollheim, W. M., Buffam, I., Findlay, S. E. G., Hall, R. O., Jr., Hotchkiss, E. R., et al. (2016). Dissolved organic carbon uptake in streams: A review and assessment of reach-scale measurements. *Journal of Geophysical Research: Biogeosciences*, 121(8), 2019–2029. https://doi.org/10.1002/2015JG003204
- Musolff, A., Fleckenstein, J. H., Rao, P. S. C., & Jawitz, J. W. (2017). Emergent archetype patterns of coupled hydrologic and biogeochemical responses in catchments. Geophysical Research Letters, 44(9), 4143–4151. https://doi.org/10.1002/2017GL072630
- Nepf, H. (1999). Drag, turbulence, and diffusion in flow through emergent vegetation. Water Resources Research, 35(2), 479–489. https://doi.org/10.1029/1998WR900069
- Nepf, H., & Vivoni, E. (2000). Flow structure in depth-limited, vegetated flow. *Journal of Geophysical Research*, 105(C12), 28547–28558. https://doi.org/10.1029/2000JC900145
- Nepf, H. M. (2012). Hydrodynamics of vegetated channels. *Journal of Hydraulic Research*, 50(3), 262–279. https://doi.org/10.1080/00221686. 2012.696559
- Nezu, I., & Sanjou, M. (2008). Turburence structure and coherent motion in vegetated canopy open-channel flows. *Journal of Hydro-Environment Research*, 2(2), 62–90. https://doi.org/10.1016/j.jher.2008.05.003

WATERMAN AND HANSEN 23 of 25

- Nifong, R. L., & Taylor, J. M. (2021). Vegetation and residence time interact to influence metabolism and net nutrient uptake in experimental agricultural drainage systems. *Water*, *13*(10), 1416. https://doi.org/10.3390/W13101416
- Nikora, V. (2010). Hydrodynamics of aquatic ecosystems: An interface between ecology, biomechanics and environmental fluid mechanics. *River Research and Applications*, 26(4), 367–384. https://doi.org/10.1002/rra.1291
- Ocampo, C. J., Oldham, C. E., & Sivapalan, M. (2006). Nitrate attenuation in agricultural catchments: Shifting balances between transport and reaction. Water Resources Research, 42(1). https://doi.org/10.1029/2004WR003773
- O'Connor, B. L., & Hondzo, M. (2008). Enhancement and inhibition of denitrification by fluid- flow and dissolved oxygen flux to stream sediments. *Environmental Science & Technology*, 42(1), 119–125. https://doi.org/10.1021/es071173s
- Oldham, C. E., Farrow, D. E., & Peiffer, S. (2013). A generalized Damköhler number for classifying material processing in hydrological systems. Hydrology and Earth System Sciences, 17(3), 1133–1148. https://doi.org/10.5194/hess-17-1133-2013
- Philippot, L., Raaijmakers, J., Lemanceau, P., & van der Putten, W. H. (2013). Going back to the roots: The microbial ecology of the rhizosphere. Nature Reviews Microbiology, 11, 789–799. https://doi.org/10.1038/nrmicro3109
- Pinay, G., Peiffer, S., De Dreuzy, J.-R., Krause, S., Hannah, D. M., Fleckenstein, J. H., et al. (2015). Upscaling nitrogen removal capacity from local hotspots to low stream orders' drainage basins. *Ecosystems*, 18(6), 1101–1120. https://doi.org/10.1007/s10021-015-9878-5
- Rabalais, N. N., & Turner, R. E. (2019). Gulf of Mexico hypoxia: Past, present, and future. Limnology and Oceanography Bulletin, 28(4), 117–124. https://doi.org/10.1002/lob.10351
- R Core Team. (2024). R: A language and environment for statistical computing. R Foundation for Statistical Computing. Retrieved from https://www.R-project.org/
- Reay, S. D., Smith, K. A., & Edwards, A. C. (2003). Nitrous oxide emission from agricultural drainage waters. Global Change Biology, 9(2), 195–203. https://doi.org/10.1046/j.1365-2486.2003.00584.x
- Rockström, J., Steffen, W., Noone, K., Persson, Å., Chapin, F. S., III, Lambin, E. F., et al. (2009). A safe operating space for humanity. *Nature*, 461(7263), 472–475. https://doi.org/10.1038/461472a
- Rowiński, P. M., Västilä, K., Aberle, J., Järvelä, J., & Kalinowska, M. B. (2018). How vegetation can aid in coping with river management challenges: A brief review. *Ecohydrology and Hydrobiology*, 18(4), 345–354. https://doi.org/10.1016/j.ecohyd.2018.07.003
- Rudi, G., Bailly, J.-S., Belaud, G., Dages, C., Lagacherie, P., & Vinatier, F. (2020). Multifunctionality of agricultural channel vegetation: A review based on community functional parameters and properties to support ecosystem function modeling. *Ecohydrology and Hydrobiology*, 20(3), 397–412. https://doi.org/10.1016/j.ecohyd.2020.03.004
- Sabokrouhiyeh, N., Bottacin-Busolin, A., Savickis, J., Nepf, H., & Marion, A. (2017). A numerical study of the effect of wetland shape and inlet-outlet configuration on wetland performance. *Ecological Engineering*, 105, 170–179. https://doi.org/10.1016/j.ecoleng.2017.04.062
- Sehat, H., Abdolahpour, M., Jamali, M., & Ghisalberti, M. (2023). The impact of plant oscillation on dispersion in emergent aquatic canopies. Water Resources Research, 59(3), e2022WR032035. https://doi.org/10.1029/2022WR032035
- Seitzinger, S., Harrison, J., Bohlke, J., Bouwman, A., Lowrance, R., Peterson, B., et al. (2007). Denitrification across landscapes and waterscapes: A synthesis. *Ecological Applications : A Publication of the Ecological Society of America*, 16(6), 2064–2090. https://doi.org/10.1890/1051-0761(2006)016[2064:DALAWA]2.0.CO;2
- Sharp, S. J., Elgersma, K. J., Martina, J. P., & Currie, W. S. (2021). Hydrologic flushing rates drive nitrogen cycling and plant invasion in a freshwater coastal wetland model. *Ecological Applications*, 31(2), e02233. https://doi.org/10.1002/eap.2233
- Sirivedhin, T., & Gray, K. A. (2006). Factors affecting denitrification rates in experimental wetlands: Field and laboratory studies. *Ecological Engineering*, 26(2), 167–181. https://doi.org/10.1016/j.ecoleng.2005.09.001
- Soana, E., Bartoli, M., Milardi, M., Fano, E. A., & Castaldelli, G. (2019). An ounce of prevention is worth a pound of cure: Managing macrophytes for nitrate mitigation in irrigated agricultural watersheds. Science of the Total Environment, 647, 301–312. https://doi.org/10.1016/j.scitotenv. 2018.07.385
- Soana, E., Fano, E. A., & Castaldelli, G. (2018). Estimate of gas transfer velocity in the presence of emergent vegetation using argon as a tracer: Implications for whole-system denitrification measurements. *Chemosphere*, 213, 526–532. https://doi.org/10.1016/j.chemosphere.2018. 09.079
- Soana, E., Gavioli, A., Tamburini, E., Fano, E. A., & Castaldelli, G. (2018). To mow or not to mow: Reed biofilms as denitrification hotspots in drainage canals. *Ecological Engineering*, 113, 1–10. https://doi.org/10.1016/j.ecoleng.2017.12.029
- Stegen, J. C., Fansler, S. J., Tfaily, M. M., Garayburu-Caruso, V. A., Goldman, A. E., Danczak, R. E., et al. (2022). Organic matter transformations are disconnected between surface water and the hyporheic zone. *Biogeosciences*, 19(12), 3099–3110. https://doi.org/10.5194/bg-19-3099-2022
- Stevens, M., & Hoag, C. (2000). Narrowleaf cattail plant guide. USDA, NRCS, National Plant Data Center & Idaho Plant Materials Center. Retrieved from https://plants.usda.gov/DocumentLibrary/plantguide/pdf/pg_tyan.pdf
- Tamburini, E., Soana, E., Monti, M., Fano, E. A., & Castaldelli, G. (2020). Introducing life cycle assessment in costs and benefits analysis of vegetation management in drainage canals of lowland agricultural landscapes. Water, 12(8), 2236. Article 8. https://doi.org/10.3390/w12082236
- Tang, C., Yi, Y., & Zhang, S. (2023). Flow and turbulence in unevenly obstructed channels with rigid and flexible vegetation. *Journal of Environmental Management*, 326(A), 116736. https://doi.org/10.1016/j.jenvman.2022.116736
- Taylor, P. G., & Townsend, A. R. (2010). Stoichiometric control of organic carbon–nitrate relationships from soils to the sea. *Nature*, 464(7292), 1178–1181. Article 7292. https://doi.org/10.1038/nature08985
- Temkin, A., Evans, S., Manidis, T., Campbell, C., & Naidenko, O. V. (2019). Exposure-based assessment and economic valuation of adverse birth outcomes and cancer risk due to nitrate in United States drinking water. *Environmental Research*, 176, 108442. https://doi.org/10.1016/j.envres.2019.04.009
- Thomas, F., & Cornelisen, C. (2003). Ammonium uptake by seagrass communities: Effects of oscillatory versus unidirectional flow. Marine Ecology Progress Series, 247, 51–57. https://doi.org/10.3354/meps247051
- Tiedje, J. (1988). Ecology of denitrification and dissimilatory nitrate reduction to ammonium. Methods of Soil Analysis. Part 2. Chemical and Microbiological Properties, 717, 179–244.
- Truong, S. H., & Uijttewaal, W. S. J. (2019). Transverse momentum exchange induced by large coherent structures in a vegetated compound channel. *Water Resources Research*, 55(1), 589–612. https://doi.org/10.1029/2018WR023273
- Tseng, C. Y., & Tinoco, R. O. (2020). A model to predict surface gas transfer rate in streams based on turbulence production by aquatic vegetation. Advances in Water Resources, 143, 103666. https://doi.org/10.1016/j.advwatres.2020.103666
- Unigarro Villota, S., Ghisalberti, M., Philip, J., & Branson, P. (2023). Characterizing the three-dimensional flow in partially vegetated channels. Water Resources Research, 59(1), e2022WR032570. https://doi.org/10.1029/2022WR032570

WATERMAN AND HANSEN 24 of 25



Water Resources Research

- 10.1029/2023WR036995
- Walton, C. R., Zak, D., Audet, J., Petersen, R. J., Lange, J., Oehmke, C., et al. (2020). Wetland buffer zones for nitrogen and phosphorus retention: Impacts of soil type, hydrology and vegetation. *Science of the Total Environment*, 727, 138709. https://doi.org/10.1016/j.scitotenv.2020. 138709
- Wang, D., & Hejazi, M. (2011). Quantifying the relative contribution of the climate and direct human impacts on mean annual streamflow in the contiguous United States. Water Resources Research, 47(10), W00J12. https://doi.org/10.1029/2010WR010283
- Wang, Q., Liu, Q., Hu, Y., Ding, J., Ma, Q., Zong, K., & Yang, Z. (2019). Effect of carbon source derived from macrophytes on microbial denitrification in constructed wetlands: Role of plant species. *Bioresource Technology Reports*, 7, 100217. https://doi.org/10.1016/j.biteb. 2019.100217
- Ward, M. H., Jones, R. R., Brender, J. D., de Kok, T. M., Weyer, P. J., Nolan, B. T., et al. (2018). Drinking water nitrate and human health: An updated review. *International Journal of Environmental Research and Public Health*, 15(7), 1557. https://doi.org/10.3390/ijerph15071557
- Waterman, B. R., & Hansen, A. (2024). Experimental datasets used to investigate hydro- biogeochemical controls on nitrate removal at the interface of flowing water and artificial emergent vegetation. https://doi.org/10.17605/OSF.IO/ZN29W
- Welty, J., Wick, C., Wilson, & Rorrer, G. (2000). Fundamentals of momentum, heat and mass transfer (5th ed., p. 729). Wiley & Sons, Inc.
- White, B. L., & Nepf, H. M. (2007). Shear instability and coherent structures in shallow flow adjacent to a porous layer. *Journal of Fluid Mechanics*, 593, 1–32. https://doi.org/10.1017/S0022112007008415
- White, B. L., & Nepf, H. M. (2008). A vortex-based model of velocity and shear stress in a partially vegetated shallow channel. Water Resources Research, 44(1), W01412. https://doi.org/10.1029/2006WR005651
- Xia, Y., Zhang, M., Tsang, D. C. W., Geng, N., Lu, D., Zhu, L., et al. (2020). Recent advances in control technologies for non-point source pollution with nitrogen and phosphorous from agricultural runoff: Current practices and future prospects. *Applied Biological Chemistry*, 63(1), 8. https://doi.org/10.1186/s13765-020-0493-6
- Zhang, X., Song, C., Mao, R., Yang, G., Tao, B., Shi, F., et al. (2014). Litter mass loss and nutrient dynamics of four emergent macrophytes during aerial decomposition in freshwater marshes of the Sanjiang plain, Northeast China. *Plant and Soil*, 385(1), 139–147. https://doi.org/10.1007/s11104-014-2217-3
- Zhao, S., Wang, J., Feng, S., Xiao, Z., & Chen, C. (2022). Effects of ecohydrological interfaces on migrations and transformations of pollutants: A critical review. Science of the Total Environment, 804, 150140. https://doi.org/10.1016/j.scitotenv.2021.150140
- Zheng, L., Cardenas, M. B., & Wang, L. (2016). Temperature effects on nitrogen cycling and nitrate removal-production efficiency in bed form-induced hyporheic zones. *Journal of Geophysical Research: Biogeosciences*, 121(4), 1086–1103. https://doi.org/10.1002/2015JG003162

WATERMAN AND HANSEN 25 of 25